



**HAL**  
open science

## Agulhas eddy fluxes in a 1/6° Atlantic model

Anne-Marie Tréguier, Olaf Boebel, Bernard Barnier, Gervan Madec

► **To cite this version:**

Anne-Marie Tréguier, Olaf Boebel, Bernard Barnier, Gervan Madec. Agulhas eddy fluxes in a 1/6° Atlantic model. *Deep Sea Research*, 2003, II (20), pp.251-280. 10.1016/S0967-0645(02)00396-X. hal-00182381

**HAL Id: hal-00182381**

**<https://hal.science/hal-00182381>**

Submitted on 13 Jan 2020

**HAL** is a multi-disciplinary open access archive for the deposit and dissemination of scientific research documents, whether they are published or not. The documents may come from teaching and research institutions in France or abroad, or from public or private research centers.

L'archive ouverte pluridisciplinaire **HAL**, est destinée au dépôt et à la diffusion de documents scientifiques de niveau recherche, publiés ou non, émanant des établissements d'enseignement et de recherche français ou étrangers, des laboratoires publics ou privés.



Distributed under a Creative Commons Attribution 4.0 International License

# Agulhas eddy fluxes in a $1/6^\circ$ Atlantic model<sup>☆</sup>

A.M. Treguier<sup>a,\*</sup>, O. Boebel<sup>b</sup>, B. Barnier<sup>c</sup>, G. Madec<sup>d</sup>

<sup>a</sup>*Laboratoire de Physique des Océans, CNRS-Ifremer-UBO, IFREMER, BP70, 29280 Plouzané, France*

<sup>b</sup>*Alfred Wegener Institute, Bussestrasse 24, 27570 Bremerhaven, Germany*

<sup>c</sup>*Laboratoire des Écoulements Géophysiques et Industriels, BP 53, 38041 Grenoble cedex 09, France*

<sup>d</sup>*Laboratoire d'Océanologie dynamique et de Climatologie, boîte 100, 4 place Jussieu, 75252 Paris, France*

---

## Abstract

A  $1/6^\circ$  resolution primitive equation model of the Atlantic circulation is analyzed in the Agulhas region. The model has a realistic level of eddy kinetic energy, and produces anticyclonic Agulhas rings as well as cyclonic structures. In the model as well as in the data, ring trajectories undergo a transition between a turbulent character in the Cape Basin and a steady propagation in the rest of the South Atlantic. The topography of the Walvis Ridge does not seem to play a part in generating this contrast in the model. The model shows that cyclones are primarily generated from the negative shear vorticity side of the Agulhas Current as it leaves the coast, and they are most of the time paired with anticyclones in dipolar or tripolar structures. Contribution of Agulhas rings to the transports has been estimated by two methods, either focussing on the amount of water trapped inside the eddies and carried with them, or as a perturbation to the time-mean flow. The second estimate always produces smaller mass fluxes than the first. Even so, the transient eddy flux (2 Sv of warm water over the Agulhas Ridge) is very large when compared to parameterizations of eddy fluxes used in low-resolution climate models.

---

## 1. Introduction

The Agulhas retroflection, south of Africa, is one of the most energetic regions of the world ocean. To describe and quantify the fluxes resulting from eddy generation, translation and decay, a

four-dimensional picture in space and time is needed. The combination of satellite altimetry and floats (Boebel and Barron, 2003) gives us a flavor of such a picture. However, a high-resolution coverage of the region is required both in space and time, and this can be achieved by numerical models only.

The analysis of Agulhas eddies in high-resolution basin-scale models has remained somewhat superficial until now, due to the lack of realism of the early eddy-permitting models. The Fine Resolution Antarctic Model (FRAM) produced eddies that were too large, too warm and too salty, and the retroflection occurred too far east (Lutjeharms and Webb, 1995). In the limited-area model

---

\*Corresponding author.

E-mail address: treguier@ifremer.fr (A.M. Treguier).

of Biastoch and Krauss (1999) the retroflection was located  $5^\circ$  too far west. Other recent eddy-permitting models (equatorial resolution between  $1/4^\circ$  and  $1/3^\circ$ ) reproduce more faithfully the location of the retroflection loop, like the Parallel Ocean Program (POP, Maltrud et al., 1998), the SPEM sigma coordinate model (Penduff et al., 2001), or the CLIPPER  $1/3^\circ$  model ATL3 (Treguier et al., 2001), but these models fail to reach the observed amplitude of the eddy variability. Another problem in FRAM was that the Agulhas ring formation was much too regular, as demonstrated by the analysis of temperature fronts (Lutjeharms and Webb, 1995, their Fig. 8). This regularity also appears in the time series of barotropic streamfunction from ATL3 (Treguier et al., 2001, their Fig. 13). In those models, the formation of rings by pinching of the retroflection loop seems to follow the simple scenario proposed by Pichevin et al. (1999), of a retroflecting current achieving its momentum balance by shedding eddies regularly. By contrast, the sea-surface

height time-series from Modular Data Assimilation System (MODAS), Fox et al., 2001), which compare well with in-situ data (Boebel and Barron, 2003), reveal a very irregular structure of the retroflection loop, eddy formation occurring intermittently rather than with a fixed period.

A new, higher-resolution model of the Atlantic Ocean Circulation has recently been implemented as a French contribution to World Ocean Circulation Experiment (WOCE). This model configuration (referred to as ATL6) is similar to the ATL3 model of Treguier et al. (2001), except for its refined grid ( $1/6^\circ$  at the equator). Overall, the circulation is similar in ATL3 and ATL6. Problems in the representation of western boundary currents (Gulf Stream separation and Brazil-Malvinas confluence zone) exist in both models. The Agulhas retroflection region, however, is simulated differently, and more realistically, in the highest-resolution case. The time series of the barotropic streamfunction near the retroflection region (Fig. 1) is irregular in ATL6, while it is

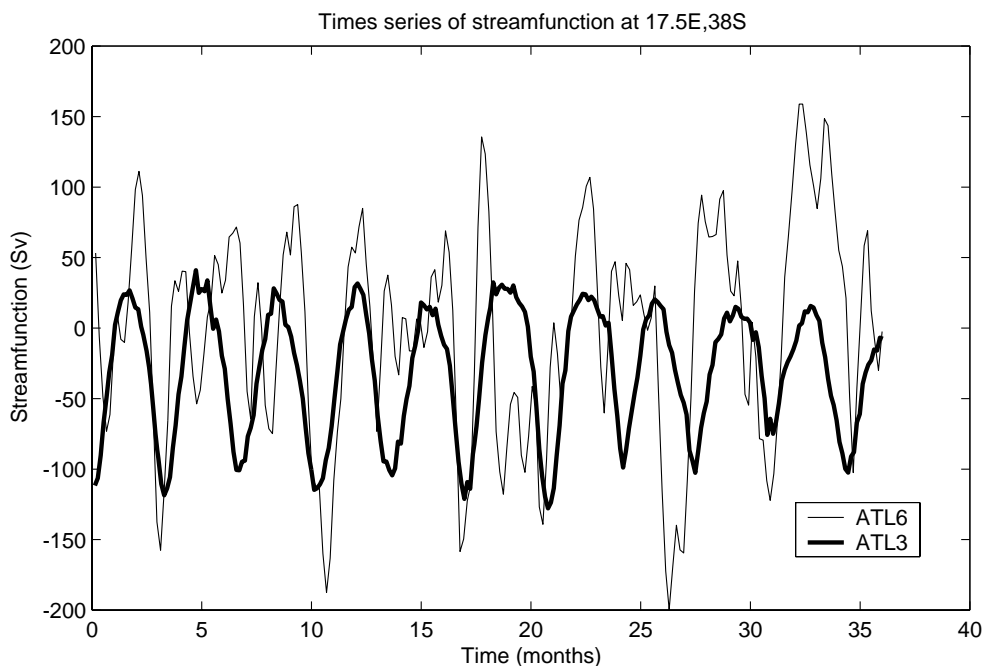


Fig. 1. Time series of barotropic streamfunction at  $38^\circ\text{S}$ ,  $17.5^\circ\text{E}$  near the Agulhas retroflection in two CLIPPER models, ATL6 ( $1/6^\circ$ ) and ATL3 ( $1/3^\circ$ ). Note that the ATL3 experiment shown here is forced by daily wind stress and fluxes, and not a climatology as in Treguier et al. (2001). This shows that the difference in character of the two series is due to the model resolution and not the forcing.

almost periodic in ATL3. Animations of sea-surface height in ATL6 are remarkably similar in character to those based on MODAS observations (electronic annexes to this issue).

Stimulated by the realistic character of the eddy formation processes, we use output from the ATL6 model to investigate the dynamics of Agulhas rings in the model and their contribution to the basin-scale fluxes. After a description of the model (Section 2), we analyze in Section 3 the model Agulhas eddies. We compare model results with the MODAS sea-surface height data, for both anticyclones and cyclones. The latter have been emphasized only recently in the observations (Boebel et al., 2003a). Our model provides a description of their formation mechanism. Section 4 examines in more detail the evolution of the anticyclones and their interaction with the topography. Finally, quantification of eddy fluxes is attempted in Sections 5 and 6. Like all high-resolution models integrated only for a few decades, ATL6 exhibits a significant drift in terms of its water mass properties: these limitations must be considered when interpreting the fluxes. We contrast in this paper two different points of view on the influence of rings on the circulation: the contribution to the fluxes of water trapped inside the rings (a quantity often estimated from data), and the transient eddy fluxes (estimated as a deviation from the time-mean in models). The analysis of ATL6 makes us skeptical about the possibility of parameterizing the interocean exchange by Agulhas eddies in low-resolution climate models.

## 2. Model description

Model configurations at various resolutions (ATL1 at  $1^\circ$ , ATL3 at  $1/3^\circ$ , and ATL6 at  $1/6^\circ$ ) have been built in the framework of the French CLIPPER project. ATL3 is described in detail in Treguier et al. (2001).

### 2.1. Model and forcing

We use the primitive equation code OPA8.1 developed at LODYC (Madec et al., 1998). It is a second-order finite difference model with a rigid lid, in  $z$ -coordinates on the vertical. The horizontal

grid is a Mercator isotropic grid with resolution  $1/6^\circ$  at the equator, covering the Atlantic ocean from Drake passage to  $30^\circ\text{E}$  and from Antarctica ( $75^\circ\text{S}$ ) to  $70^\circ\text{N}$ . The vertical grid has 42 geopotential levels, with a grid spacing of 12 m at the surface and 200 m below 1500 m.

A horizontal biharmonic operator is used for lateral mixing of tracers and momentum, with a coefficient varying as the third power of the grid spacing (thus the Reynolds number at grid scale is constant with latitude). The vertical mixing of momentum and tracers is calculated using a second-order closure model (Madec et al., 1998). In case of static instability the vertical mixing coefficients are set to a very large value ( $1 \text{ m}^2 \text{ s}^{-1}$ ).

The bathymetry is calculated from Smith and Sandwell (1997). Buffer zones are defined in the Norwegian Sea, Baffin Bay, and Weddell sea. There are four open boundaries at Drake passage ( $68^\circ\text{W}$ ), at  $30^\circ\text{E}$  between Africa and Antarctica, at  $8^\circ\text{W}$  in the Gulf of Cadiz and at  $70^\circ\text{N}$  beyond the sills of the Nordic seas. A detailed description (algorithm and behavior) of the open boundaries in the South Atlantic is found in Treguier et al. (2001). The last two open boundaries exist only in the ATL6 configuration (CLIPPER, 2000); they use the same numerical algorithm, and their details are not essential to the present paper. The model is initialized using the seasonal climatology of Reynaud et al. (1998). The integration starts in the northern hemisphere winter season (February 15th). Seasonal values of temperature and salinity are interpolated linearly in time to serve as relaxation fields in the buffer zones. The surface forcing fields are derived from the ECMWF reanalysis ERA-15. The heat flux is formulated as suggested in Barnier et al. (1995), using their feedback coefficient for relaxation to the Reynolds SST field. The evaporation minus precipitation ( $E-P$ ) fluxes are formulated as a pseudo salt flux, including river run-off (Treguier et al., 2001).

### 2.2. Open boundary at $30^\circ\text{E}$

Since the eastern open boundary lies very close to the retroreflection region, it is important to recall its characteristics. The model solution at the open boundary is the sum of two terms, a radiation and

a relaxation to climatology. An Orlanski-type phase velocity is estimated using a few grid points next to the boundary and the previous time steps (Barnier et al., 1998). When the phase velocity is outbound, the solution is calculated by a radiation equation from the interior solution; when the phase velocity is inbound, the solution is calculated by strong relaxation to a prescribed climatology (with a characteristic time of one day). The detailed analysis of Treguier et al. (2001) has shown that the radiative velocity estimated this way is not physical; at every grid point along the boundary (regardless of the presence of strong eastward or westward currents) the phase velocity is inbound 50% of the time. This means that the solution at the boundary remains always close to the climatology.

Special care has been taken to calculate a boundary climatology at  $30^{\circ}\text{E}$ . Because the model has a high resolution, we chose to use a WOCE synoptic section (WOCE I6, Park et al., 2001), taken in February–March 1996. The temperature and salinity from the data have been smoothed near  $36^{\circ}\text{S}$  to remove a large cold eddy that was observed during the cruise, and may not be a permanent feature. The baroclinic zonal velocity is estimated from geostrophy, but the model needs the absolute velocity. In previous models of the South Atlantic with open boundaries (Barnier et al., 1998 for instance) an analytical function was used to define the barotropic streamfunction. In an attempt to make barotropic and baroclinic components of the velocity compatible with each other, we have first estimated the barotropic transport by geostrophy with a reference level at the bottom. The resulting streamfunction (which gives a total circumpolar transport of 325 Sv) has been adjusted linearly in different latitude ranges to fit estimates from data. We chose to impose an inflow of 70 Sv in the Agulhas Current, an inflow of 15 Sv in the Weddell gyre, and a total circumpolar transport of 140 Sv. These inflow quantities are constant in time because we have no data to prescribe time variability at the boundary. Consequently, the seasonal variability near the boundary is biased, and there is no perturbation coming from the Indian Ocean. Such perturbations have been linked to the formation of Natal pulses, which in turn may trigger Agulhas eddy

shedding in the real ocean (Lutjeharms et al., 2003). It is interesting to note that ATL6 achieves quite a realistic eddy formation with a constant inflow of the Agulhas Current.

### 2.3. Model integration

The model is spun-up during 8 years using a repeated seasonal forcing cycle (average of the years 1979–1993 of the ECMWF reanalysis). From the end of the spin up, the model is integrated over the years 1979–1993 (15 years) using the daily forcings of the reanalysis. The experiment is pursued over the years 1994–2000 using the ECMWF analysis winds and fluxes. During the last 20 years of the experiment 5-day averages of the model variables are stored for diagnostic purposes. We concentrate the present analysis on the most recent years of the model integration (1995–1999).

This paper discusses the model solution in the South Atlantic and the Agulhas region. Other aspects will be discussed elsewhere, and are highlighted in a report (CLIPPER, 2001). The meridional heat flux is about 0.4 PW at  $30^{\circ}\text{S}$  and 0.9 PW at  $20^{\circ}\text{N}$ , with significant interannual variability. The meridional overturning streamfunction is about 16 Sv at  $40^{\circ}\text{N}$ . A plot of model eddy kinetic energy (EKE) compared with EKE derived from TOPEX (Ducet et al., 2000) shows that the level of surface EKE reached in the model in the Agulhas is similar to observations (Fig. 2). The Malvinas–Brazil confluence zone is too far south in the ATL6 model. The POP global ocean model (resolution of  $0.28^{\circ}$ , Maltrud et al., 1998) showed a similar behavior. This problem could be due to an insufficient model resolution; in the North Atlantic, refining the horizontal grid has been shown to improve considerably the separation of the Gulf Stream from the coast (Smith et al., 2000).

## 3. Agulhas eddies in the Cape Basin

### 3.1. Computing eddy trajectories

One could conceive several ways to define Agulhas eddies in the model, using vorticity or

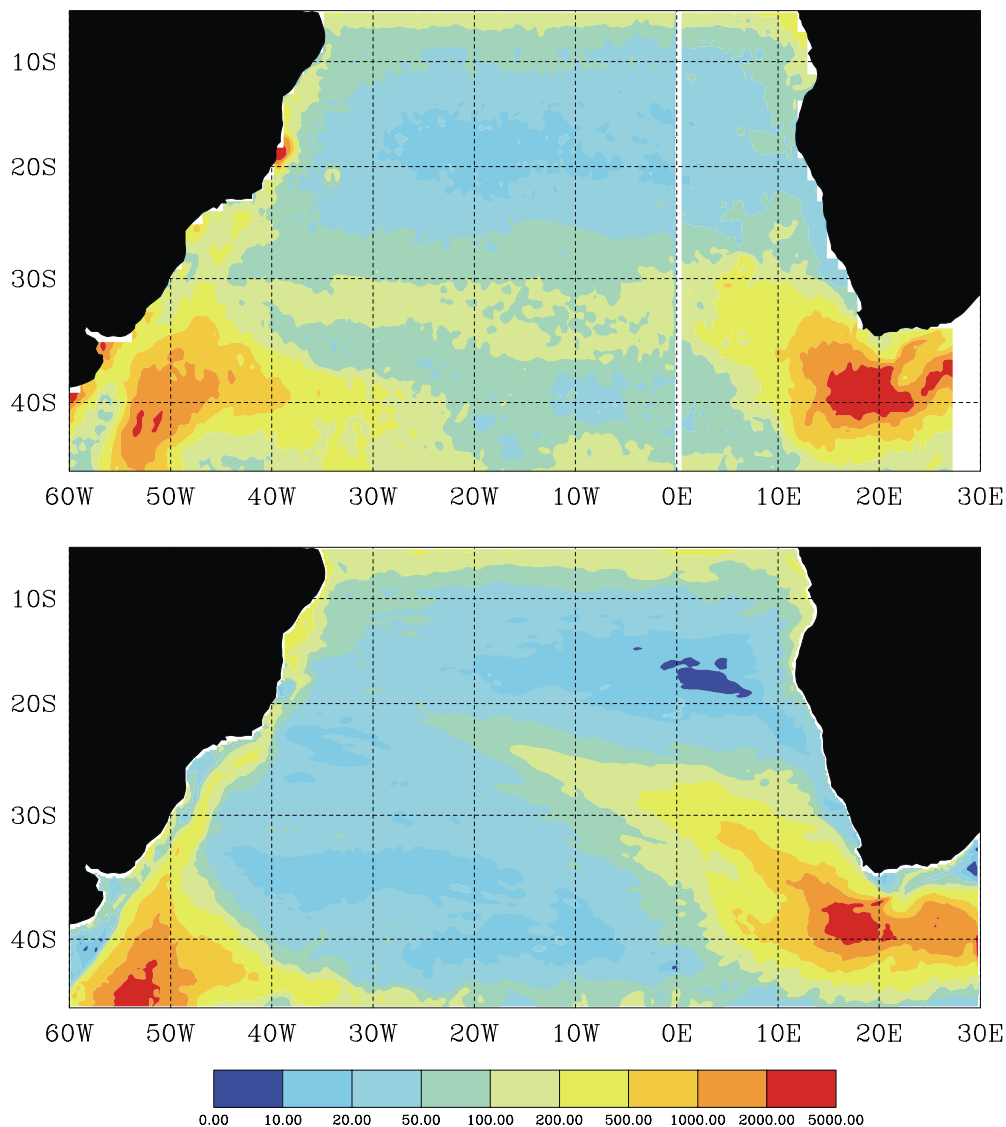


Fig. 2. Maps of surface eddy kinetic energy ( $\text{cm}^2 \text{s}^{-2}$ ) in the South Atlantic. Top: calculation from TOPEX-ERS data over the period 1992–1997 (Ducet et al., 2000), Bottom: ATL6 model over the same period.

isopycnal height anomalies. We choose a criterion based on the sea-surface height (SSH) anomaly relative to the time-mean, because this quantity is observed by satellite altimetry. Near the retro-reflection region between  $10^\circ\text{E}$  and  $20^\circ\text{E}$ , the flow is extremely turbulent. Animations of relative vorticity (see also Fig. 5) show the formation of

anticyclones of various sizes as well as cyclonic filaments and eddies. Those structures strongly interact, merge or break up. We have thus found convenient to define anticyclonic and cyclonic structures as they cross the  $10^\circ\text{E}$  meridian, and calculate their trajectories forward and backward from this point.

We define as anticyclonic rings the anomalies greater than 0.4 m at 10°E. This ensures that all the long-lived rings are captured. This choice results in seven rings crossing 10°E in 1995, five in 1996, six in 1997, three in 1998 and six in 1999. Those numbers agree roughly with the analysis of Schouten et al. (2000) based on TOPEX altimeter data: they find five rings in 1995 and 1996, and six rings in 1994. Cyclones have a weaker signature on the SSH, so we define them as negative anomalies greater than -0.25 m at 10°E. With this criterion we identify 11, 4, 8, 2, and 3 cyclonic structures for the years 1995–1999.

Our forward (backward) tracking algorithm is quite primitive, but well suited to model outputs (characterized by no measurement error nor missing data). It consists in finding for each snapshot of SSH the maximum value in a square of  $13 \times 13$  grid points around the location of the maximum SSH at the previous (or next) time step. Once identified at 10°E, the eddies are tracked backward in time until they reach 19°E, which we consider as their formation region. They also are tracked forward in time from 10°E until the SSH anomaly falls below 0.05 m, or until they merge with a newer eddy. No interpolation in space or time is performed. The eddy positions have the spatial resolution of the model grid and the temporal resolution of the archived dataset (5 days); more frequent snapshots would be needed for a more precise tracking. In order to consider only complete trajectories we restrict the analysis to eddies defined in 1995, 1996 and 1997. The trajectories of the 18 selected anticyclones are from 55 to 1010 days long, with an average of 775 days. Similarly, 23 cyclonic structures are tracked for an average of 305 days (from 70 to 800 days).

A slightly different approach was taken to track eddies in the MODAS absolute steric SSH field (Fox et al., 2001). Note that only the MODAS SSH field is used in this paper; this field is based on data from the TOPEX/POSEIDON altimeter and does not contain model information excepted for a SSH climatology added to the satellite variability. Details of the tracking routine are given in Boebel et al. (2003a). Eddy locations are based on the continuous existence of local SSH extrema for at

least 4 months, allowing for a maximal gap of 30 days and associated inter-maxima distances of less than 100 km. The number of anticyclones observed in MODAS is comparable to ATL6. We classify the anticyclones by year as they cross 5°E (this longitude is chosen instead of 10°E in order to keep a few long-lived eddies formed in 1996 in the MODAS dataset). With this criterion we find 3, 3 and 4 anticyclones in 1997, 1998 and 1999, respectively. These numbers are a lower limit, since modifications of the detection parameters produces somewhat higher numbers (by one or two). The difficulty results from the seasonal, steric heaving of the sea-surface, as well as the spatial variability of the climatological SSH used to define the MODAS SSH. The maximum duration of a trajectory is 781 days, and the average 421 days.

Cyclones in MODAS decrease in intensity more rapidly than the anticyclones so that a minimum of 2 months has been chosen for the tracking routine, resulting in the detection of 22 cyclones in 1997 (some of which may have formed in 1996), 24 in 1998 and 16 in 1999. Using this same criterion for anticyclones results in 8, 6 and 4 anticyclones for 1997, 1998 and 1999. The smaller number of anticyclones in the southwestern Cape Basin is thus robust in this dataset. MODAS cyclones are tracked for a maximum time of 395 days, and average time of 182 days.

### 3.2. *Anticyclones trajectories*

The trajectories of anticyclonic rings in the model and in MODAS are represented in Fig. 3. Striking similarities exist between the two. Most noticeable is the qualitative difference between the trajectories in the Cape Basin and after Walvis Ridge.

While in the Cape Basin, the model anticyclones remain in its southern part. This confinement of rings south of 30°S in the Cape Basin is consistent with the maps of surface eddy kinetic energy derived from altimetry (Fig. 2) and the analysis of observations by Goñi et al. (1997). On the contrary, a significant number of the rings observed by Schouten et al. (2000) crossed the

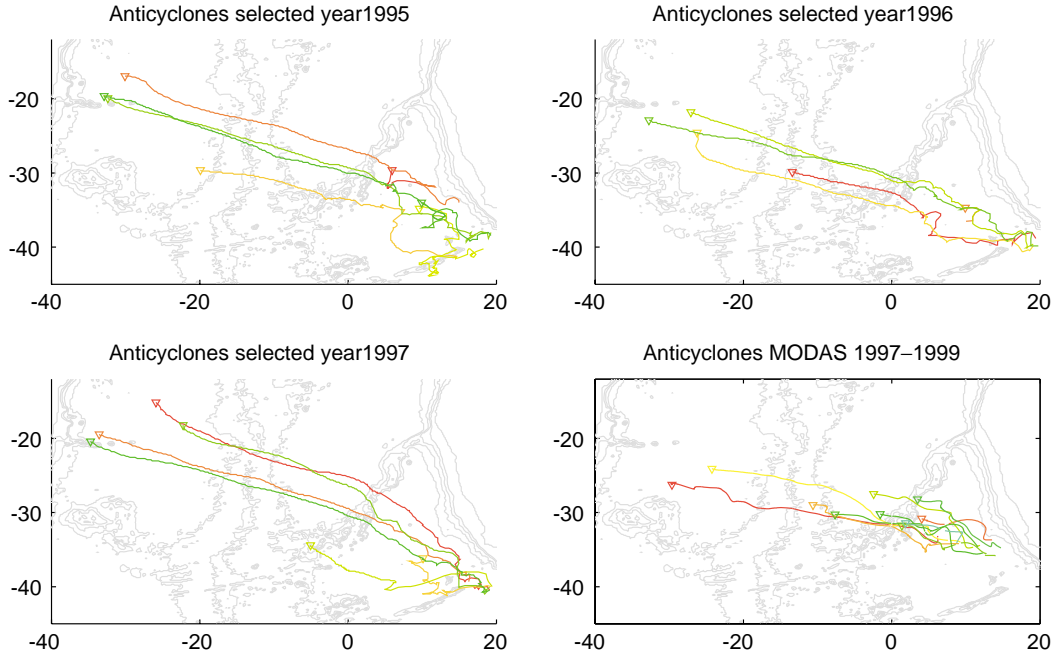


Fig. 3. Upper panels and lower left: trajectories in the ATL6 model of selected Agulhas rings that crossed the longitude  $10^{\circ}\text{E}$  during years 1995, 1996 and 1997, respectively. Lower right: trajectories in MODAS of selected anticyclones that crossed  $5^{\circ}\text{E}$  between 1997 and 1999. The  $5^{\circ}\text{E}$  longitude has been preferred for MODAS to include two long trajectories of eddies formed in 1996.

$10^{\circ}\text{E}$  meridian north of  $30^{\circ}\text{S}$  (1 out of 5 or 6). These authors found that most rings with northern trajectories resulted from eddy splitting events. From a total of 21 newly formed rings, Schouten et al. (2000) identified 13 rings resulting from splitting (over a four year period), bringing their total to 34. In our case, many splitting events can be identified in the Cape Basin near the formation area, but they rarely lead to the formation of two distinct long-lived eddies. Most of the time, the eddies resulting from the split merge again after one or a few months, so we have not considered them in our census.

The MODAS trajectories, like the model ones, remain confined in the southern part of the Cape Basin. This may be due to interannual variability (Schouten et al. considered years 1993–1996) or a different treatment of the altimeter data and different detection algorithm. A single analysis covering a long period is needed to address this question.

### 3.3. Cyclones trajectories

Fig. 4 shows the trajectories of the cyclonic structures in the model and in MODAS. Note that for MODAS, only cyclones that crossed  $10^{\circ}\text{E}$  are included in the figure, for a better comparison with the model. In contrast with the anticyclones, those structures rarely leave the Cape Basin, and have much more irregular trajectories.

In the model, inspection of SSH animations reveals that the structures are not coherent eddies but rather, most of the time, elongated structures and filaments associated with the anticyclones. We have inspected maps of relative vorticity at the time when each cyclonic structure is defined at  $10^{\circ}\text{E}$ . Out of the 23 structures, we would loosely define 12 as being part of a dipolar structure (in association with an anticyclone); 3 as being part of a tripolar structure (an anticyclone flanked by 2 cyclones), 6 as filaments, and only 2 as isolated cyclones. In most cases an anticyclonic ring is

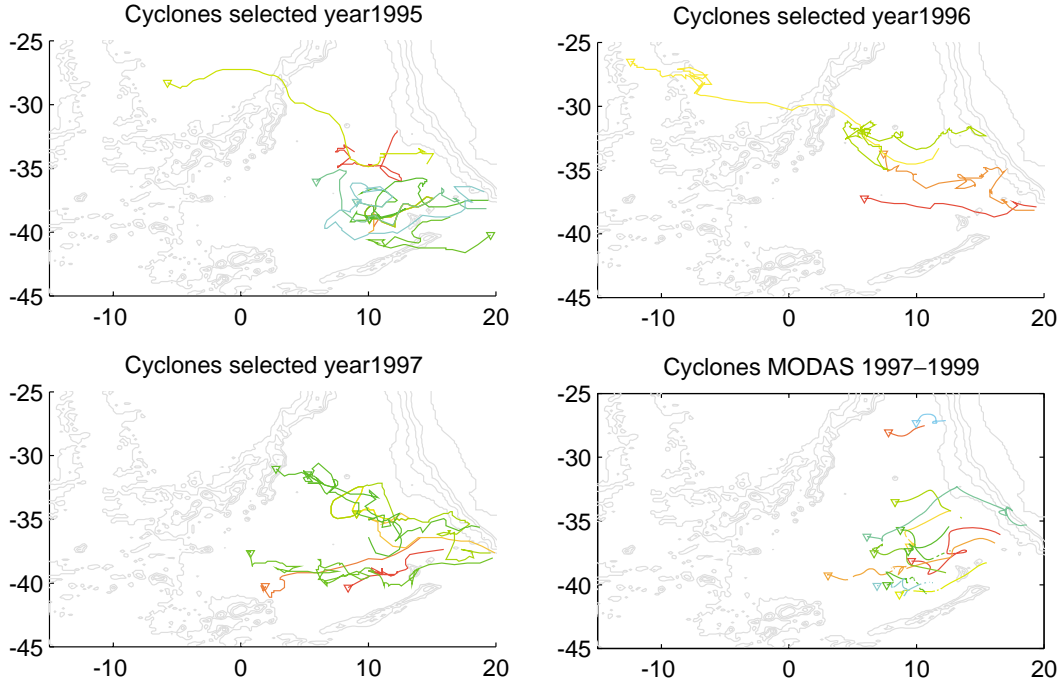


Fig. 4. Upper panels and lower left: trajectories in the ATL6 model of selected cyclonic structures that crossed  $10^{\circ}\text{E}$  during years 1995, 1996 and 1997, respectively. Lower right: trajectories in MODAS of selected structures that crossed  $10^{\circ}\text{E}$  between 1997 and 1999.

surrounded by at least 2 minima of negative vorticity; when the 2 minima have similar strength we classify the structure as a “tripole”, while when 1 minimum is dominant we tend to view it as a “dipole”. In both cases the positive vorticity extremum (the Agulhas ring) is larger than the negative extrema. Such a dipolar structure appears near  $14^{\circ}\text{E}$ ,  $37^{\circ}\text{S}$  in Fig. 5. The formation of multipolar structures is expected from the non-linear instability of vortices (see, for example, Carton and Legras, 1994). The presence of weak cyclones accompanying anticyclonic rings has been first suggested by Garzoli et al. (1996). These authors noted a “recoil effect” at the passage of an eddy (the isopycnals rising around an anticyclone above their depth in the far field). Arhan et al. (1999) further identified this phenomenon with the presence of cyclonic vorticity. Indeed, this behavior is ubiquitous in the model and it is characteristic of the dipolar and tripolar structures.

In the MODAS trajectories, some cyclonic eddies remain trapped at the western coast of Africa. Those are not reflected in the ATL6 trajectories because we have defined the model cyclones at  $10^{\circ}\text{E}$ . The larger cyclone to anticyclone ratio in MODAS and the dominant southwestward propagation (as opposed to the northwestward propagation in ATL6) could also be due to the definition of the cyclones in the model. There is southwestward propagation of some negative vorticity patches in ATL6 (as seen from animations of model results in the Cape Basin). Although the data (like the model) show a difference between the life time of cyclones and anticyclones, Lagrangian trajectories and MODAS SSH both suggest that the cyclones are often axisymmetric structures (like the anticyclones). This could be an indication that the cyclones are less stable in the model than in reality. We do not feel that a more quantitative and precise comparison is possible at this time, both

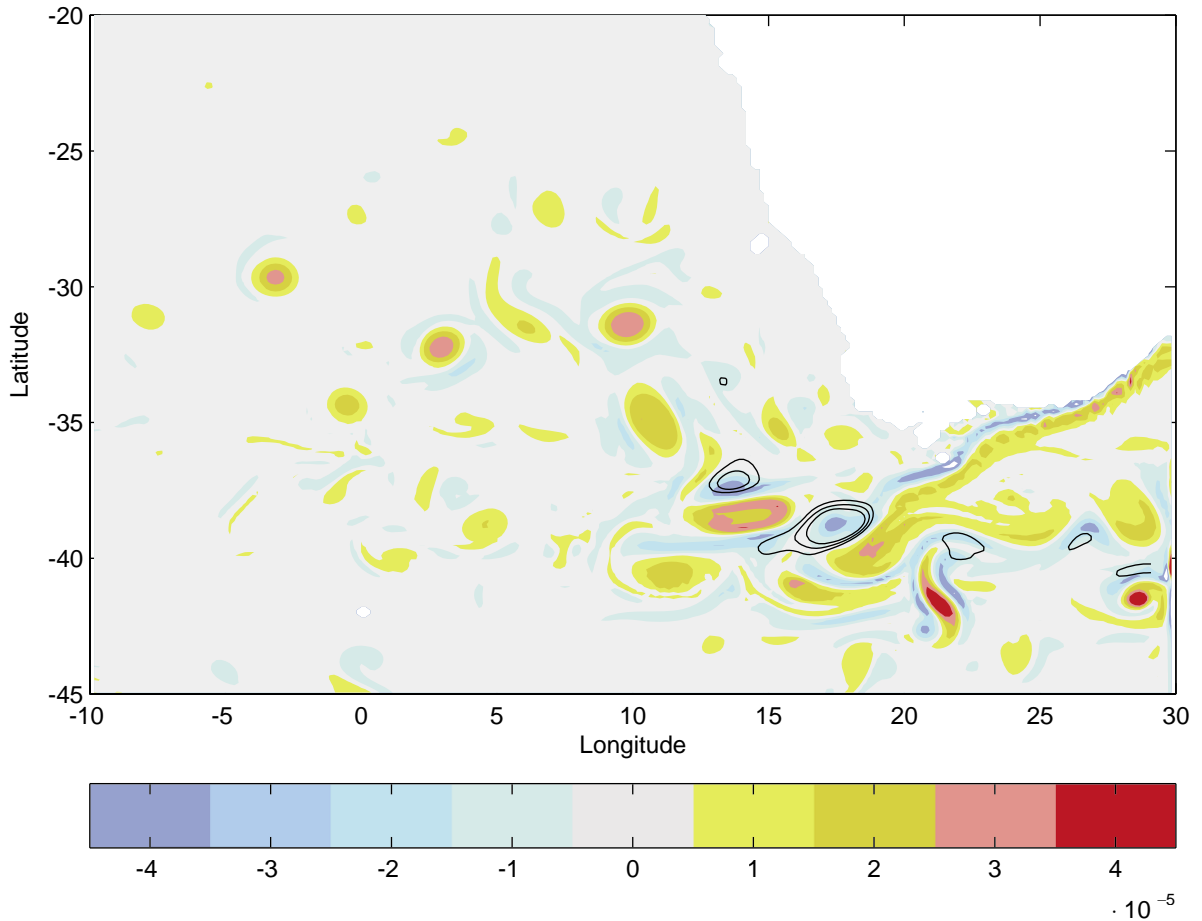


Fig. 5. Instantaneous field of relative vorticity ( $\text{s}^{-1}$ ) on May 9th, 1997 at 96 m depth in the ATL6 model. The black contours indicates areas (cyclones) where the sea-surface height anomaly is below  $-30$  cm (contours  $-30$ ,  $-40$  and  $-50$  cm are indicated).

because of the difficulty of tracking cyclones in the data and because of the marginal resolution of those features by the ATL6 model.

We do believe, however, that ATL6 sheds light on the origin of the cyclones. Almost all the model cyclones can be traced back to the negative shear vorticity region on the north side of the Agulhas Current. An instantaneous map of relative vorticity shows that in the region east of  $10^{\circ}\text{E}$ , the maximum negative vorticity is often more intense than the positive (Fig. 5). Cyclonic eddy formation most often occurs where the Agulhas Current separates from the shelf (one large cyclone just formed in this manner appears in Fig. 5 at  $18^{\circ}\text{E}$ ).

The generation process often follows the scenario investigated by Penven et al. (2001), similar to instability of a flow past a topographic feature. However, formation of cyclones by axisymmetrization of a negative vorticity filament also occurs farther south, either at the tip of the retroflection, or even in the Agulhas return current. Animations also show the occasional formation of dipole pairs which then propagate rapidly toward the southwest.

With their limited area model, Penven et al. (2001) could only study the initial formation of a cyclone, and not its long-term evolution. Our model suggests that the strong cyclones that form

in the retroreflection loop area very quickly break up or decay, and do not show any tendency for merging (as opposed to anticyclones). The difference between the life time of cyclones and anticyclones seem realistic in view of the MODAS data. The dynamical processes that are responsible for this asymmetry of behavior will need special investigation. On one hand, many theoretical studies point out that cyclones are less stable than their anticyclonic counterparts; but on the other hand, Gulf Stream cold-core rings are observed to be very stable (Dewar and Killworth, 1995; Dewar et al., 1999). The cyclone/anticyclone asymmetry observed in our model and in the MODAS SSH may be due to the different properties of the eddies as they form, or to their interaction after their formation.

### 3.4. Eddy amplitude

The evolution of the amplitude of the rings after their formation (Fig. 6) can be compared to the estimate of Schouten et al. (2000) from altimetry

(their Fig. 3). The model warm rings seem more intense at birth with a SSH anomaly of 0.6 m (compared with 0.45 m for Schouten et al.). Their amplitude remains stable, on average, during the first 3 months. This period is followed by a rapid decay (25 cm in 7 months) of the same amplitude as the decay observed by Schouten et al. for the first 7 months of their trajectories. A slower decay (twice slower) follows in the model. By contrast, the rings observed by Schouten et al. retain their amplitude (around 0.2 m) after the initial decay. The amplitude of SSH anomalies for cyclonic features also is indicated; most of the cyclones decay in 6 to 10 months.

A Rossby number has been calculated along the eddy trajectories as a function of the relative vorticity  $\zeta$  at the eddy center near the surface (at 96 m),  $R_0 = \zeta/2f$  ( $f$  being the Coriolis frequency). The factor of 2 has been introduced because for a gaussian eddy, this estimate of the Rossby number equals the more usual one based on the eddy maximum velocity  $V$  and the radius of maximum velocity  $L$ :  $R_0 = \zeta/2f = V/fL$ . In the model, the

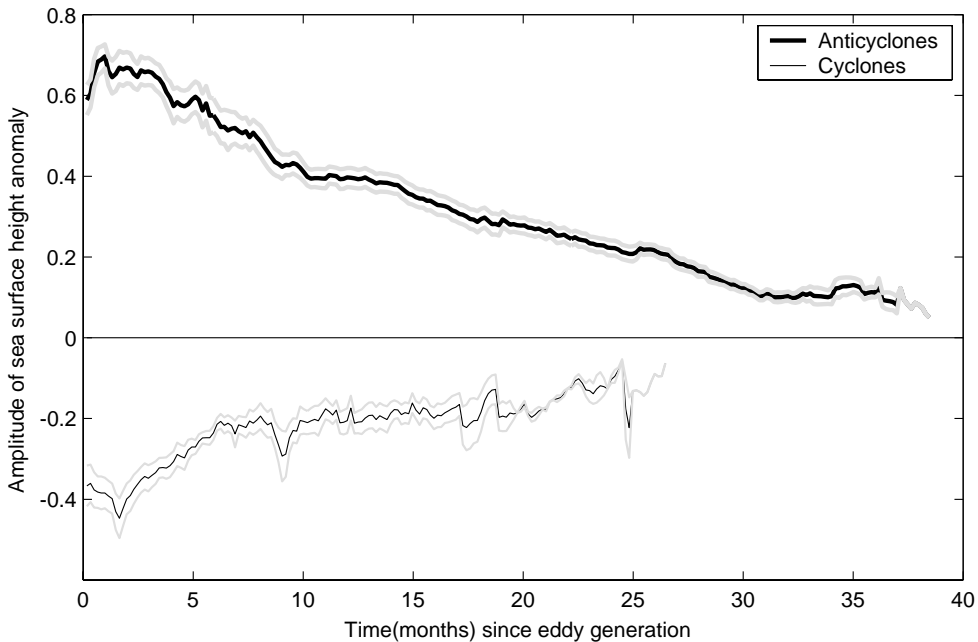


Fig. 6. Evolution of the SSH anomaly of the anticyclones and cyclones, as a function of time since the eddy formation. Grey curves indicates intervals of one standard deviation.

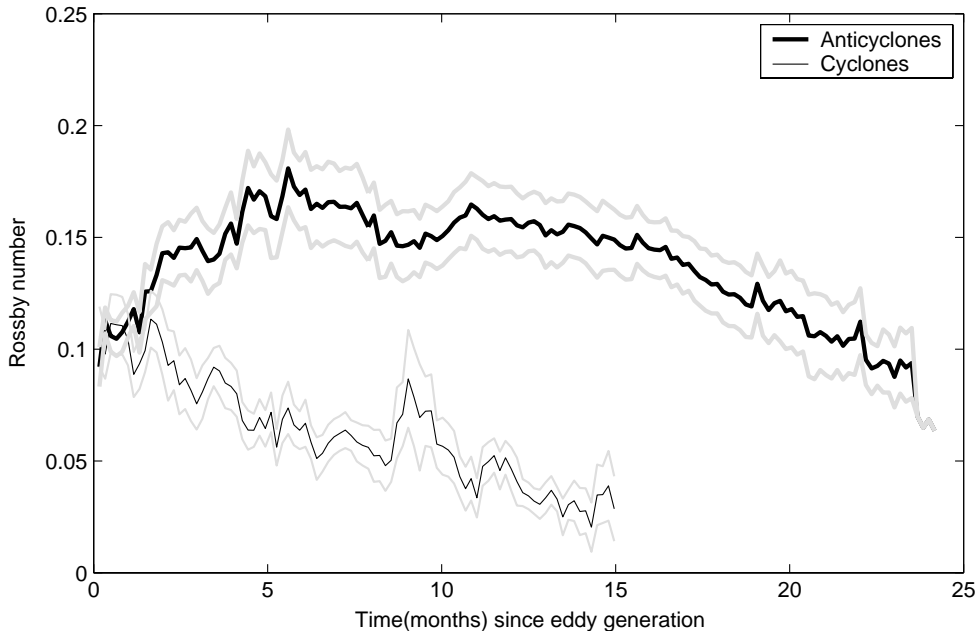


Fig. 7. Evolution of the Rossby Number of the anticyclones and cyclones as a function of time since the eddy formation. Grey curves indicates intervals of one standard deviation.

Rossby number of the rings is around 0.15, which corresponds to the upper range of estimates from data. Schmid et al. (2003) find a Rossby number of 0.08–0.21 in a mature ring using surface drifter data. Olson and Evans (1986), Garzoli et al. (1999) and Mc Donagh et al. (1999) have smaller estimates (0.04–0.07; 0.05–0.07, and 0.09–0.13, respectively). The large Rossby number of the model rings near the surface, together with the large SSH anomaly of the rings at birth, suggest that either the model rings are too strong, or their surface signature is overestimated (the vertical structure is described in more detail in the following section).

Surprisingly, the Rossby number of anticyclones grows during the first months (Fig. 7). This growth of about 60% is only partly (20%) due to the equatorward movement of the rings. The rest is due to an increase of relative vorticity. Rings could increase their relative vorticity while conserving their potential vorticity if they deepen; this increase may be a peculiarity of the definition of the Rossby number chosen here. This region being

very turbulent, a more precise investigation of the behavior of individual eddies is very complex.

#### 4. Anticyclone evolution after leaving the Cape Basin

##### 4.1. The rings structure

In the model it is possible to follow the three-dimensional structure of eddies with time, but this is quite a daunting task, complicated by the fact that the eddies are not perfectly axisymmetric. As a first estimate of eddy structure parameters we have chosen to consider the anticyclones of Fig. 3 as they cross two sections: 10°E in the Cape Basin and 10°W outside the Cape Basin. Eddy properties at those two sections are summarized in Table 1. The structure of cyclones is not considered in detail. It is more difficult to characterize in an automated fashion because in a dipole (or tripole) the velocity varies continuously from one vorticity center to the next. Cyclones tend to be weaker

Table 1

Statistics for anticyclonic eddies at two sections for rings selected during years 1995, 1996 and 1997

Property	10°E section	10°W section
Number of Agulhas rings	17	12
Maximum absolute velocity (m/s)	0.83 (0.18)	0.45 (0.08)
$\delta v$ (m/s)	0.04 (0.18)	0.08 (0.03)
Maximum velocity at 450 m (m/s)	0.54 (0.11)	0.28 (0.06)
Depth of maximum velocity (m)	30 (13)	66 (47)
Depth of maximum shear (m)	240 (115)	239 (107)
Radius of maximum velocity (km)	104 (23)	82 (8)
Core potential temperature	17.7 (0.96)	17 (0.86)
Core salinity	35.56 (0.12)	35.65 (0.09)
Barotropic/total kinetic energy	0.43 (0.13)	0.35 (0.10)

The first number is the average, the standard deviation is indicated between braces.  $\delta v$  is the difference between the absolute values of the maximum and minimum velocities across the ring, and the radius of maximum velocity is half the average of their distance. A nonzero  $\delta v$  may be due to the ring advection by the mean flow or the ring asymmetry. The ratio of barotropic over total kinetic energy is defined in the core region (within the maxima of velocity on each side of the eddy center).

(maximum velocities of order  $20 \text{ cm s}^{-1}$  at  $10^\circ\text{E}$ ) and smaller in size than anticyclones.

The comparison of the two sections (Table 1) confirms the strong decay of the anticyclonic rings between  $10^\circ\text{E}$  and  $10^\circ\text{W}$ : the maximum azimuthal velocity decreases by 46%. The difference  $\delta v$  between the absolute maxima of positive and negative velocity along the section can be due to eddy asymmetry or to the advection velocity (superimposed onto the eddy swirl velocity). Near the generation area (the  $10^\circ\text{E}$  section),  $\delta v$  is less than 10% of the maximum velocity for half the rings; for some of them,  $\delta v$  reaches 25%. At  $10^\circ\text{W}$ , we note that the negative velocity (northern side of the eddy) is always larger in absolute value than the positive velocity, in agreement with the systematic advection toward the west. At  $10^\circ\text{W}$  all rings have similar  $\delta v$  of order 18% (the standard deviation of this quantity is much smaller at  $10^\circ\text{W}$  than at  $10^\circ\text{E}$ ). The eddy radii show a similar behavior: while rings at  $10^\circ\text{E}$  have a wide range of sizes (radii ranging from 64 to 166 km) the ones that reach  $10^\circ\text{W}$  have all similar sizes

(radii from 74 to 92 km). The rings are very barotropic at  $10^\circ\text{E}$ , the barotropic energy being on average 43% of the total kinetic energy in the eddy core. This percentage decreases to 35% on average at  $10^\circ\text{W}$ , although individual rings may become more barotropic (it is the case for 4 out of 12 eddies).

The velocities and sizes of the model anticyclones compare well with observations. It is not so for the depth of maximum shear. The model’s average of 240 m seems small compared with the values of 750–950 m cited by Garzoli et al. (1999). The depth of maximum shear does not give a good idea of the penetration of a ring in the model, because the velocity steadily decreases from the near-surface layers (Fig. 8). The maximum velocity at 450 m ( $0.28 \text{ m s}^{-1}$  at  $10^\circ\text{W}$ ), as well as the isopycnal displacement around 800 m (not shown) compare well with the rings R2 and R3 found by Arhan et al. (1999) at that longitude; the model profiles fit reasonably with data from their ring R2 (Fig. 8). However, none of the model rings reproduce the subsurface maximum above a large vertical shear observed in Arhan et al.’s rings R1 and R3 (see also Garzoli et al., 1999). Certainly, a vertical mixing mechanism in the eddy cores is missing in the model. Arhan et al. (1999) underline the importance of wintertime convection in homogeneizing the rings. This process may be misrepresented in the model due to an inadequate specification of surface fluxes; we have not found any very cold eddy similar to ring R1 of Arhan et al. (1999), with core temperature lower than  $12^\circ\text{C}$ . We have defined the “core” temperatures and salinities in Table 1 as the properties at the center of the ring and at the depth of maximum shear. Temperatures tend to be high because that depth is relatively shallow. However, even accounting for the depth at which we measure  $T$ , the model eddies do seem too warm by about  $1^\circ\text{C}$ .

#### 4.2. Effect of the Walvis Ridge

To leave the Cape Basin, Agulhas anticyclones must cross the Walvis Ridge. The influence of this major topographic feature on the rings is somewhat controversial. For example, van Ballegooyen

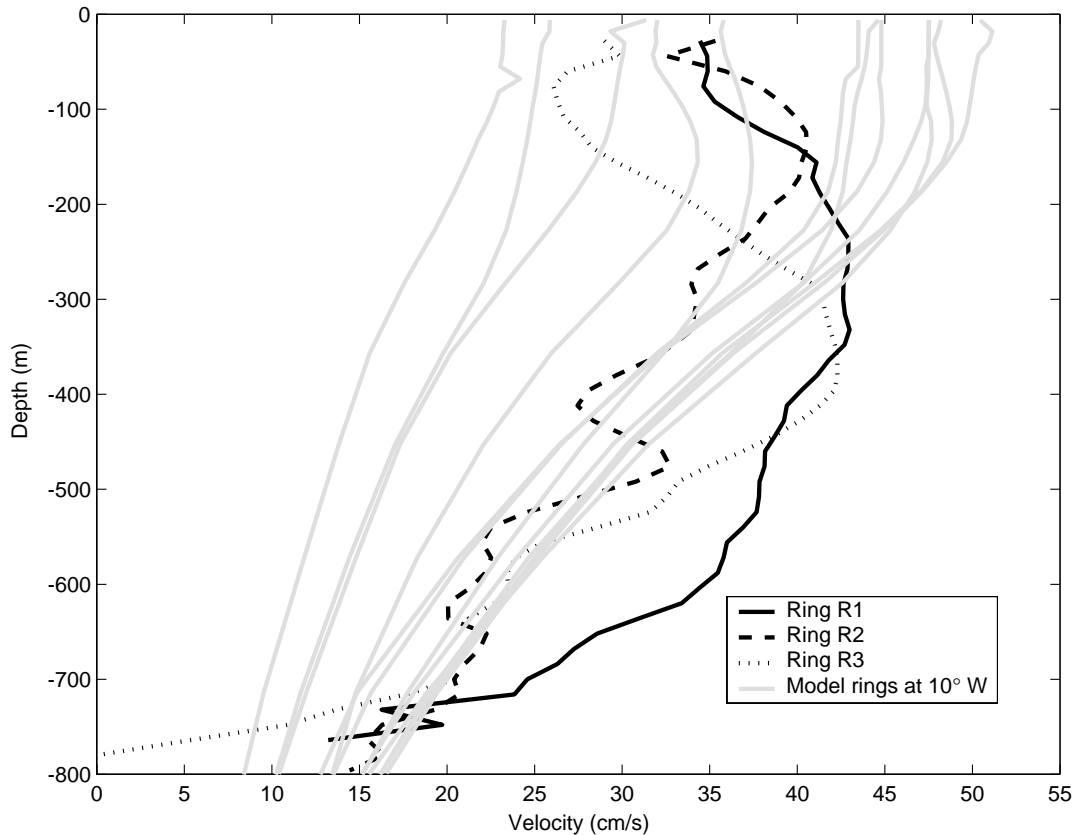


Fig. 8. Vertical profiles of azimuthal velocity in the model Agulhas rings (12 rings crossing  $10^{\circ}\text{W}$ , grey curves) and in the three rings observed by Arhan et al. (1999, their Fig. 6). Observed profiles are from acoustic doppler current profiler. Ring R1 was observed at  $39.5^{\circ}\text{S}$ ,  $11^{\circ}\text{E}$ , ring R2 at  $31.5^{\circ}\text{S}$ ,  $9^{\circ}\text{W}$  and ring R3 at  $26^{\circ}\text{S}$ ,  $9^{\circ}\text{W}$ . The profiles in the figure are calculated at each depth by averaging the maximum and minimum velocities along the section across the ring.

et al. (1994) found one ring that slowed down before crossing the ridge and decayed more rapidly during the process. However, in a global study of 39 rings, Schouten et al. (2000) found no systematic effect directly related to the ridge. They noted a decrease of the velocity as the eddies go westward, which could be due to spatial variations of the advecting field. The analysis of the altimetric measurements by Schouten et al. did not allow them to investigate the effect of topography on the eddy shape (calculations of eddy diameter being too noisy). Using a two-layer numerical model, Kamenkovich et al. (1996) found that the SSH anomaly increased by about 0.1 m just before

crossing the ridge. Using a two-layer idealized quasigeostrophic model, Beismann et al. (1999) found no increase of SSH at the crossing of the ridge by an anticyclonic eddy, but they emphasized the equatorward deflection of the trajectory induced by the ridge. Schouten et al. (2000) found evidence of those two effects (increase in SSH and northward deflexion), but only for few of the rings considered. On the contrary, Garnier et al. (2002) emphasize the role of topography, in a study based on the same altimetry data as Schouten et al., but after assimilating the data into a quasi-geostrophic model. The discrepancy between the two studies may come from the influence of the model

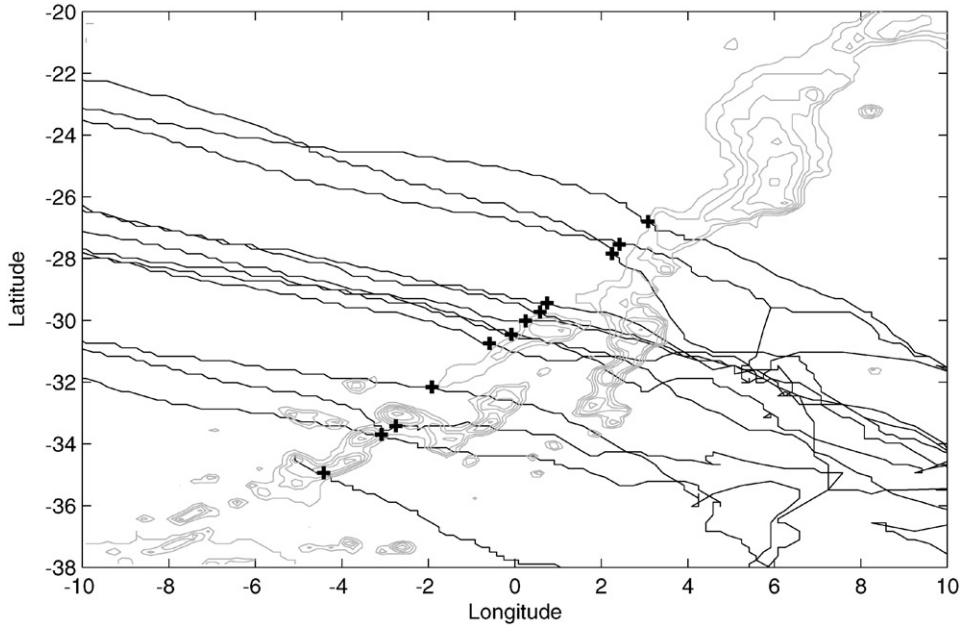


Fig. 9. Zoom of the trajectories of the anticyclones in Fig. 3 as they cross Walvis Ridge. The crosses indicate our definition of the time of crossing. Contours indicate bathymetry shallower than 3500 m (contour interval 500 m). Wiggles in the trajectories are due to the resolution of the model SSH ( $1/6^\circ$  in space, 5 days in time). No interpolation has been performed.

dynamics on the trajectories after assimilation, or from the fact that Garnier et al. (2002) examine in detail only five eddies out of Schouten's total of 39.

There does not seem to be any systematic effect of the Walvis Ridge on the rings in our primitive equation model. A map of the ring trajectories in the vicinity of the Walvis Ridge is shown in Fig. 9. Eddy paths are not systematically deflected to the North as suggested by Beismann et al. (1999). Some rings decay substantially while crossing the ridge, mainly those to the south. Others decay much less or even slightly intensify (Fig. 10). All theoretical studies have suggested that the eddies should become more baroclinic as they cross Walvis Ridge. Besides the SSH, Fig. 10 also shows the evolution of the barotropic streamfunction as the rings cross the ridge. The evolution is very similar to the SSH and shows no systematic decrease at crossing.

In fact, the most obvious signal in Figs. 9 and 10 is the difference in character of the trajectories between the Cape Basin and the Angola Basin

already mentioned in the previous section: in the Cape Basin trajectories are turbulent and eddy properties vary widely, while trajectories are linear and ring properties more uniform in the Angola Basin. Likely, this is the consequence of eddy–eddy interactions, which are particularly intense in the Cape Basin (nearby the rings generation area), and tend to decrease as rings take their own route to the west.

Our conclusion (the lack of proof for a systematic effect of Walvis Ridge on the model rings) is in sharp contrast with the POPCM model results of Matano and Beier (2003). It is not easy to understand the difference between the two models because it is quantitative rather than qualitative. In ATL6 as in POPCM, cyclones are mostly confined to the Cape Basin. A plot of cyclonic and anticyclonic kinetic energy in ATL6 (not shown) is very similar to Matano and Beier's Fig. 9, and the barotropic eddy energy has a weak maximum near the location of Vema Seamount in both models. There is more barotropic energy in

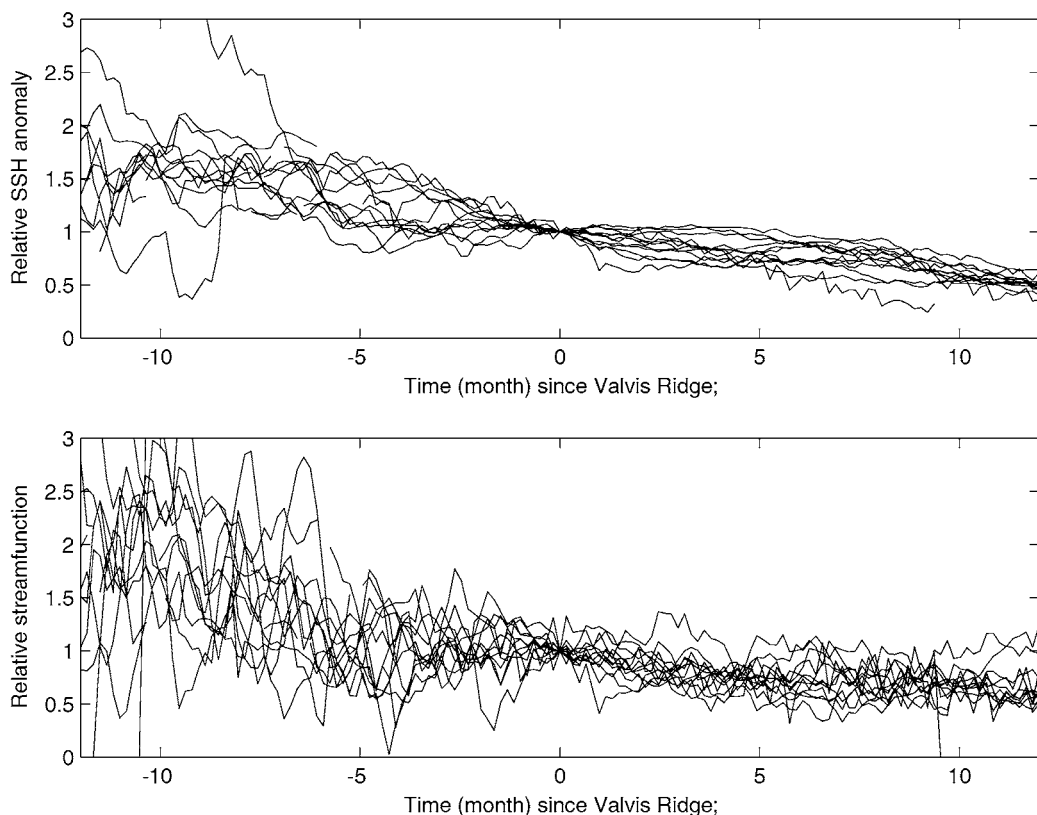


Fig. 10. Evolution of the SSH anomaly and streamfunction of the rings as a function of the time of crossing Walvis Ridge. Both quantities are normalized for each eddy by the value at the time of crossing.

the rings generation region in ATL6 than in POCM, and bottom-intensified cyclones as pictured in Matano and Beier's Fig. 13 are also found in the ATL6 model. Both ATL6 and POCM are  $z$ -coordinate models, which represent topography as a series of staircases. Such a representation may underestimate topographic influence; could this defect be accentuated as the vertical resolution increases (which is the case between POCM and ATL6)? We hope that a more detailed comparison of the two models can bring answers to this question.

#### 4.3. Agulhas rings propagation

After leaving the Cape Basin the eddies decay slowly, and propagate at a nearly constant speed.

A map of the propagation velocity is drawn (Fig. 11) by averaging the velocities along the eddy trajectories in  $5^\circ$  bins. The average velocity is about  $6 \text{ cm s}^{-1}$ , quite similar with the velocities from Schouten et al. (2000) and Garnier et al. (2002). There is also remarkable agreement with a new estimate based on MODAS giving for the zonal and meridional propagation  $c_x = -5.2 \text{ cm s}^{-1} (\pm 1.6)$  and  $c_y = 1.7 \text{ cm s}^{-1} (\pm 1.2)$ . The ATL6 model values are  $c_x = -5.4 \text{ cm s}^{-1}$  and  $c_y = 1.9 \text{ cm s}^{-1}$ . Advection by the mean flow is generally pointed out as being the main source of eddy displacement. The model allows us to compare the eddy drift  $(c_x, c_y)$  with the time-mean Eulerian velocities  $(u, v)$  at 227 m, depth at which the rms difference between the two velocity fields is minimum. The model eddy drift is substantially

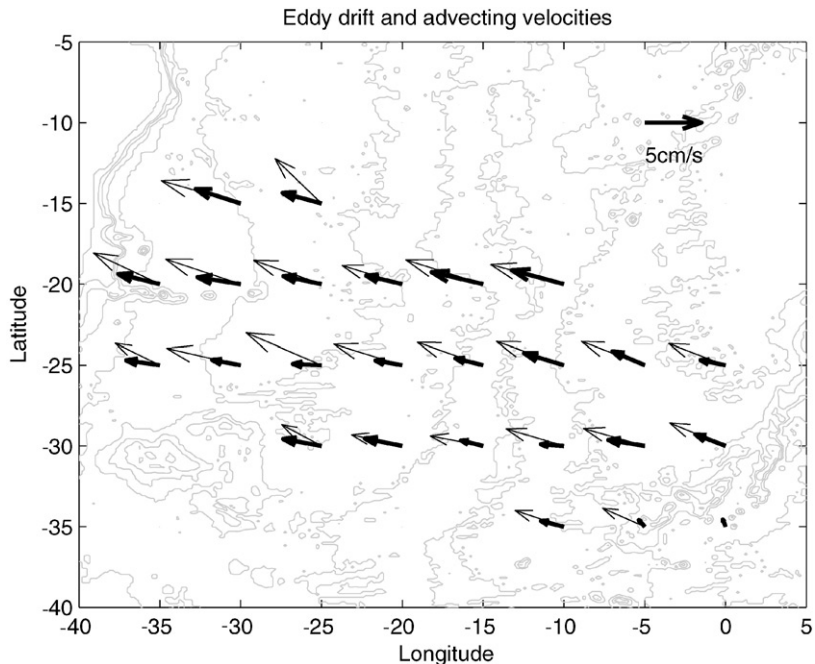


Fig. 11. Velocities of the center of anticyclones, estimated from the trajectories and averaged in  $5^\circ$  bins (thin arrows); time-mean Eulerian velocities of the model at 227 m, averaged in the same bins (thick arrows).

larger than the advection velocity. The extra velocity to the west can be accounted for by the eddy self-propagation due to the  $\beta$  effect. We have estimated the  $\beta$  drift using the formula of Olson and Evans (1986), based on a shallow water approximation and assuming an axisymmetric shape of our eddies; we obtain values ranging from  $0.01$  to  $0.05 \text{ m s}^{-1}$ , compatible with the difference between  $c_x$  and  $u$  in Fig. 11. The excess northward propagation, relative to advection, is consistent with the equatorward propagation of nonlinear anticyclones. However, vortices much larger in size than the Rossby radius have a small equatorward self-advection compared to their  $\beta$ -induced westward propagation (Mc Williams and Flierl, 1979), and it should be the case for Agulhas rings.

The model Agulhas rings reach the western basin ( $30^\circ\text{W}$ ) around  $20\text{--}25^\circ\text{S}$ . Their path is more to the north than found by Schouten et al. (2000), even more north than the paths of the eddies

studied by Garnier et al. (2002), but it could be compatible with the trajectories calculated from MODAS for years 1997–1999. The discrepancy between the maps of surface eddy kinetic energy from altimetry and in the model (Fig. 2) probably reflects this tendency for the model rings to drift too far north after crossing Walvis Ridge. One possible reason for an exaggerated northward motion is the vertical structure of the model eddies. If the eddies were deeper, they would be advected by a more westward mean flow because of the structure of the South Atlantic subtropical gyre (the center of the gyre moves to the south with increasing depth). Another possibility is the lack of influence of Walvis Ridge in the ATL6 model, because the eddies of Matano and Beier (2003), which seem more influenced by topography, have a more realistic trajectory outside the Cape Basin. Model comparisons and process studies in the parameter range of Agulhas rings could help resolve this issue in the future.

## 5. The nature of eddy fluxes

### 5.1. Definitions

The ATL6 model has been shown to produce a realistic number of eddies (both cyclones and anticyclones), a good first approximation of their structure, and the right level of eddy kinetic energy. It is thus a valid tool to estimate the relative eddy contribution to fluxes of volume, heat and salt (although the total fluxes must be interpreted with care, see next section). An annual mean “eddy” flux can be estimated from two points of view:

- The “trapped” eddy flux,  $F_t$ . It is estimated by considering the volume, heat or salt anomaly of one eddy, multiplying it by the drift velocity, and taking into account the number of eddies per year. The underlying assumption is that the eddies are sufficiently nonlinear so that the anomalies are trapped inside their core, down to a “trapping depth”.
- The “transient” eddy flux,  $F'$ . This is the classical estimate in turbulence theory. Eddies are considered as deviations from an average; an ensemble average is the most appropriate but a time-average is generally used due to the lack of available ensemble statistics. The transient mass flux in an isopycnal layer,  $\overline{v'h'}$ , is estimated as the product of the perturbation velocity  $v'$  and the perturbation thickness  $h'$  of the isopycnal layer.

The first point of view has generally been adopted when analyzing data (for instance, van Ballegooyen et al., 1994, or more recently Sparrow et al., 2002). The second point of view is used in model analysis and in theoretical work on eddy parameterizations. Regarding the latter, a large emphasis has been put in the last decade on the transient mass flux  $\overline{v'h'}$ , or rather the eddy-induced (or “bolus”) velocity  $v^* = \overline{v'h'}/\bar{h}$  (Gent et al., 1995).

It is important to realize the difference between the “transient” eddy flux  $F' = \overline{v'h'}$  and the “trapped” eddy flux  $F_t$ . Let us consider gaussian eddies advected by a uniform velocity across a section. The mass fluxes  $F'$  and  $F_t$  can easily be

integrated along the section, using the two methods. In that case,  $F'$  is zero while  $F_t$  is not.  $F'$  vanishes by symmetry: for each eddy there is an exact cancellation between positive and negative velocities as the eddy crosses a section.  $F_t$  is simply the product of the mean advective velocity by the averaged mass anomaly of an eddy; it is entirely captured in the time-mean flux  $\bar{F} = \bar{v}\bar{h}$  with no contribution from transients. One may ask whether larger transient eddy fluxes could be expected for self-advected eddies on a  $\beta$ -plane, since as shown in the previous section the  $\beta$  effect accounts for about half the westward velocity of the Agulhas anticyclones. We are not aware of any investigation of this question. Using the shallow water model of Pichevin et al. (1999) in an open-channel configuration, we generated a geostrophically balanced gaussian eddy with parameters adequate for the Agulhas region and let it evolve for 1 year. The eddy propagated westward as expected, and produced a negligible transient eddy flux across a meridional section. A general study of the self-advecting eddy case would have to take into account different eddy shapes and parameter ranges, and is beyond the scope of this paper.

By this simple example, we want to point out the non-local aspect of transport by coherent vortices. Transient eddy fluxes are expected to occur in the areas of eddy generation and eddy decay, but not necessarily in between. Symmetric eddies advected by a uniform background flow do not generate any eddy-induced velocity or transient eddy flux, but produce a significant “trapped” flux.

To compare the two points of view, we evaluate eddy contributions in the ATL6 model using both methods along two sections: a meridional section at 0°W, and a zonal section extending across the width of the South Atlantic basin at 30°S. We have defined four isopycnal ranges (Table 2). Results

Table 2  
Definition of the density classes for transports calculations

Surface water (SW)	$\sigma_0 < 27$
Intermediate water (IW)	$\sigma_0 > 27 \quad \sigma_1 < 32.15$
Deep water (DW)	$\sigma_1 > 32.15 \quad \sigma_4 < 45.87$
Bottom water (BW)	$\sigma_4 > 45.87$

are not very sensitive to the limits defining the deep water ( $\sigma_1 = 32.15$ ) and the bottom water ( $\sigma_4 = 45.87$ ). On the other hand, the relative transport of surface and intermediate water varies according to the limit one chooses. We have taken  $\sigma_0 = 27$ , as in Schmid et al. (2000) which produces lower transports of intermediate water compared with Rintoul (1991) inverse calculation (who used  $\sigma_0 = 26.8$ ).

To follow accurately the time variation of transports in density classes in our  $z$  coordinate model, we have found necessary to interpolate linearly the transport to the depth of each isopycnal. In the deep ocean, the model vertical

grid spacing is 200 m. The eddy and seasonal fluctuations of density cause vertical displacements of the isopycnals that are smaller than the vertical grid size. This would create noise in the time series if the transport in the model grid cells was simply binned into density classes without vertical interpolation.

### 5.2. $0^\circ W$ meridional section

A time series of warm-water transport ( $\sigma_0 < 27$ ) along the section is presented in Fig. 12. The transport is generally westward (negative), with a cumulated value from  $15^\circ S$  reaching 27.7 Sv at

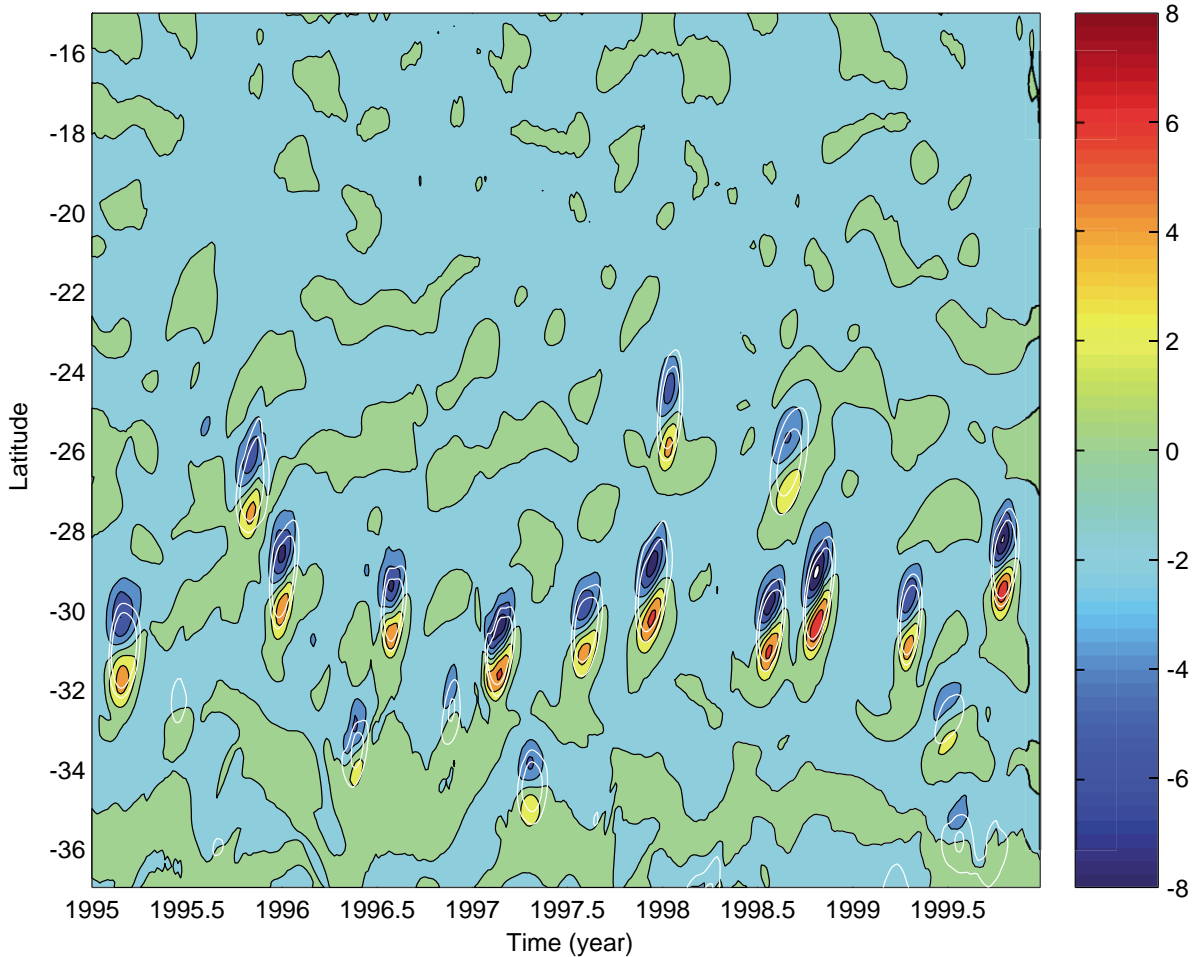


Fig. 12. Time-latitude plot of transport of warm water ( $\sigma_0 < 27$ ) along the longitude  $0^\circ W$ . Colors indicate transport (Sverdrups). The two white contours outline the regions where the perturbation depth of isopycnal  $\sigma_0 = 27$  is greater than 50 m and 100 m, respectively.

Table 3

Mass transports through two sections in density classes (see definitions in Table 2)

Mass flux (Sv)	0°W section			30°S section		
	$F$	$F_t$	$F'$	$F$	$F_t$	$F'$
Warm water (WW)	-27.7	-2.4 (1.8)	-0.2	11.0	7.6 (4.8)	2.0
Intermediate water (IW)	-7.5	-0.9 (-0.6)	0.05	1.9	4.5 (2.8)	-0.5
Deep water (DW)	5.9		0.1	-17.5		-0.7
Bottom water (BW)	0.6		-0.03	3.6		-0.8
Total depth	-28.7			-1.0		

For the 0°W section, transports are integrated from 37°S to 15°S only. For the 30°S sections, transports are integrated over the basin; the total of -1 Sv is the prescribed transport through Bering Strait.  $F$  is the total transport  $\overline{vh}$  averaged during years 1995–1999.  $F_t$  is the transport integrated on points at which the perturbation depth  $h'$  of the  $\sigma_0 = 27$  isopycnal exceeds  $h_c = 70$  m (anticyclones); the transport for  $h_c = 100$  m is added (between braces).  $F'$  is the transient eddy component ( $\overline{v'h'}$ ).

the center of the subtropical gyre (37°S at this longitude). Agulhas rings are the dominant signal in the variability. On the time-latitude diagram (Fig. 12) each eddy is characterized by an increased westward transport on its northern side (reaching 8–10 Sv of warm water) and an eastward transport to the south. Because the eddies propagate to the west, the negative velocities are larger than the positive velocities, resulting in an increased westward *mean* flow between 28°S and 30°S.

For a steady, circular eddy the trapped water parcels are those with swirl velocity exceeding the eddy propagation velocity. However, floats seeded in the core of Agulhas eddies can be quickly expelled (Schmid et al., 2003), showing this simple criterion does not apply to rings in strong interaction with cyclones and filaments. A rigorous calculation of the “trapped” eddy flux  $F_t$  would involve detailed Lagrangian calculations that cannot be performed with our database of 5-day snapshots. Therefore, we simply define  $F_t$  as the contribution to the transport for points at which the perturbation depth (relative to the time-mean) of the isopycnal  $\sigma_0 = 27$  is larger than a given value  $h_c$ . Two contours (50 and 100 m) of perturbation depth are indicated in white on Fig. 12. Those contours are close together and clearly outline the anticyclones; however the precise choice of  $h_c$  changes results quantitatively

so that calculations for two values of  $h_c$  (70 and 100 m) are indicated in Table 3. The “trapped” eddy flux is estimated for the warm water and the intermediate water, because in those layers one may assume that the water is effectively trapped inside the eddy, at least to some extent.

The “trapped” eddy flux of warm water (around 2 Sv, Table 3) is relatively weak compared to the background. There are approximately three eddies per year crossing this section. Such a flux per eddy per year ( $F_{1e} = 0.7$  Sv) corresponds to a volume  $V_{1e} = 21 \times 10^{12}$  m<sup>3</sup> for an average eddy, using the simple estimate  $F_{1e} = V_{1e}/T_y$ ,  $T_y$  being the duration of the year. This agrees qualitatively with the eddy size in the model. The “transient” eddy flux  $F'$  is negligible (Table 3), and so are the transient fluxes of heat and salt. This shows that the model eddies at 0°W behave as symmetric eddies simply advected by the mean flow.

### 5.3. 30°S zonal section

Surprisingly, the trapped eddy flux is more than twice as large across 30°S (7.6 Sv with  $h_c = 70$  m), whereas the eddies have about the same size, and the same number of eddies per year is observed as in the meridional section. This difference depends on the criterion chosen to evaluate the trapped flux; for instance, a criterion based on sea-surface height (anomaly larger than 0.1 m) gives trapped

fluxes closer to each other at  $0^\circ\text{W}$  (1.9 Sv) and  $30^\circ\text{S}$  (2.4 Sv). The difference is partly explained by the fact that about half the trapped flux at  $30^\circ\text{S}$  happens east of  $0^\circ\text{W}$  and is related to eddies in strong interaction with each other.

This, and the large amplitude of the transient eddy flux (2 Sv), demonstrates that eddies have a more complex behavior across this section, and are not simply advected northward. Associated with the transient eddy flux of warm water is a significant eddy contribution to the heat transport:  $0.11^\circ\text{PW}$  out of a total of  $0.44^\circ\text{PW}$  at  $30^\circ\text{S}$ , 25% of the total. Transient fluxes have a similar importance at  $35^\circ\text{S}$  but become very small north of the path of the Agulhas rings (at  $25^\circ\text{S}$ ), suggesting that this meridional transient flux is due to the rings themselves. This is confirmed by Fig. 13, which shows the warm water flux accumulated from the east. Both the transient and “trapped” flux  $F_t$  vary only in the east, where strong Agulhas rings cross the section. The curves

of cumulated heat transport integrated over the total depth (not shown) are similar in shape to the mass transport of warm water.

We leave for further study a precise investigation of the origin of the large transient eddy flux at  $30^\circ\text{S}$ . It may be linked with baroclinic instability of the rings, because rings simulated in the shallow water model of Pichevin et al. (1999) fail to produce significant values of  $F'$  (baroclinic instability is not allowed in a model with only one active layer). Another possible cause is the ring–ring interaction causing non-uniform translation velocities and ring deformation. Whatever the origin of  $F'$ , we find interesting to discuss its magnitude in the context of eddy parameterizations. With a section length of  $6 \times 10^6$  m, the eddy thickness flux associated with  $F'$  at  $30^\circ\text{S}$  is  $\overline{v'h'} = 0.3 \text{ m}^2 \text{ s}^{-1}$ . The mean thickness of the warm water is decreasing northward because  $30^\circ\text{S}$  is to the north of the center of the subtropical gyre. The eddy thickness flux thus happens to be locally

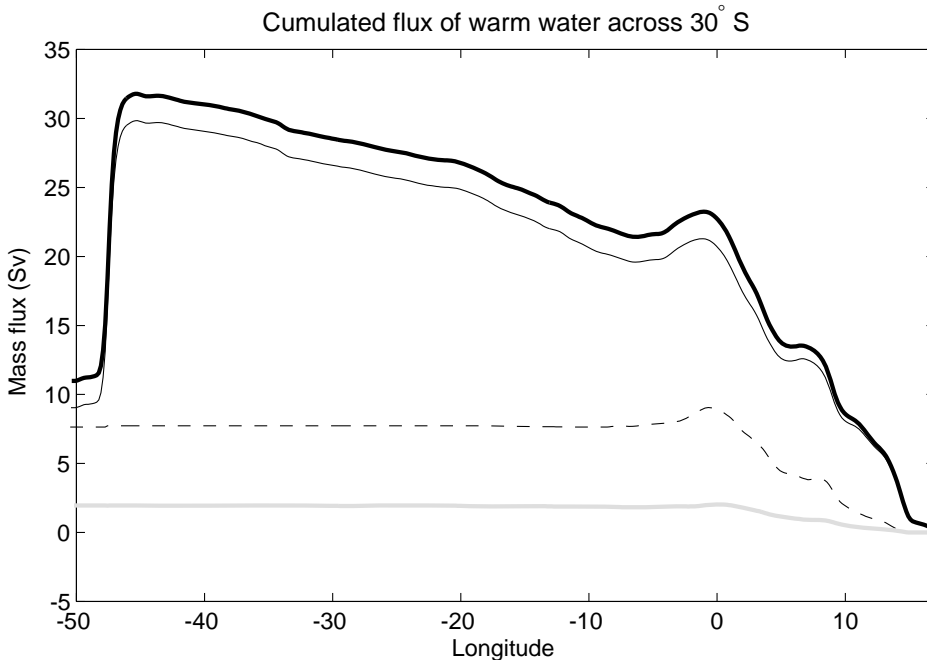


Fig. 13. Transport of warm water ( $\sigma_0 < 27$ ) cumulated from the eastern boundary along  $30^\circ\text{S}$ . The thick black curve is the total flux  $\overline{v\bar{h}}$  integrated over the section and averaged over years 1995–1999; the thin black curve the flux by the time-mean flow ( $\overline{v\bar{h}}$ ), the grey curve the transient eddy flux ( $\overline{v'h'}$ ), and the dashed curve the “trapped” flux  $F_t$  (defined using  $h_c = 70$  m, see text).

downgradient, as assumed in the parameterization of Gent et al. (1995), hereafter GM. However, if we tried to model the flux as a thickness diffusion according to GM, a very large coefficient  $\kappa$  would be necessary. GM propose that

$$\kappa = -\frac{\overline{v'H'}}{\bar{h}_y}.$$

At 30°S the meridional thickness gradient for the surface water layer, estimated from climatology, is  $\bar{h}_y = 3 \times 10^{-5}$ . Therefore a mixing coefficient  $\kappa = 10\,000 \text{ m}^2 \text{ s}^{-1}$  would be necessary to achieve the eddy bolus flux measured in ATL6. This is one order of magnitude larger than the values currently used in coarse resolution models for the GM parameterization. A local parameterization like GM necessarily fails to represent Agulhas eddies because their transport is extremely non-local (there is no reason to expect a relationship between transient fluxes and the mean gradient at 30°S, because the eddies are not generated there). A calculation for the zonal eddy-induced velocity  $u^*$  near the retroflection is not satisfying either, because the zonal gradient of the climatological isopycnal depth changes sign near 20°E. In the generation area, barotropic mechanisms are important (Pichevin et al., 1999) and baroclinic instability alone cannot explain the eddy variability.

## 6. Regional balances in the Cape Basin

The ATL6 model allows us to calculate precisely balances of mass, heat and salt in any domain bounded by grid lines. We have chosen to estimate balances in the Cape Basin, in a box bounded by three sections (Fig. 14): a section along the Agulhas Ridge designated as “Agulhas Ridge” in the tables; a section along Walvis Ridge to the North (“Walvis Ridge”) and a section closing the box, labelled “west”. This box is meant to capture the inflow of waters originating in the Indian ocean (through the Agulhas Ridge section), the inflow of subtropical South Atlantic water through the “west” section, and the outflow above Walvis Ridge of waters mixed and transformed in the “Cape Cauldron”. The box extends down to

45°S, which may seem too far south for a box lying in the subtropical gyre. However, the gyre boundary is shifted poleward in the model, as shown by the contours of barotropic streamfunction on Fig. 14. We also present two summary figures for the circulation of warm and intermediate waters, one (Fig. 15) separating the flow into “trapped flux” and “background” (the background being the total flux minus the trapped flux), and the other (Fig. 16) separating the flow into “time-mean” and “transient flux”.

### 6.1. Water mass balance

Let us consider first the mass balance (Table 4). The total mass circulating in the Cape Basin is 30.6 Sv, which is high compared with the Sverdrup transport (15 Sv integrated from the tip of Africa to 5°W along 34°S, using the model wind stress forcing). The model transport may be enhanced relative to the Sverdrup transport for physical reasons (nonlinear processes and eddy rectification, or topographic effects). We note that it does not seem overestimated compared to Garzoli et al. (1996) estimate for the Benguela Current (20–25 Sv at 30°S): the model barotropic transport at the Greenwich meridian at 30°S is only 19 Sv.

The division of the model transport across Walvis Ridge between warm and intermediate water (about 3/4 and 1/4, respectively) is in agreement with Sloyan and Rintoul (2001), who publish inverse estimates of transport at 30°S east of the Greenwich meridian (their Fig. 6). These authors find 19.8 Sv of surface water and subantarctic mode water, corresponding to our warm water (25 Sv) and 5.8 Sv of intermediate water (8.7 Sv in ATL6). On the other hand, Schmid et al. (2000) estimate that 13 Sv of intermediate water cross Walvis Ridge. We note that in both Sloyan’s inverse model and ATL6, the solution must be consistent over the whole water column while Schmid’s estimate considers only the intermediate water.

There is a large recirculation across the model Agulhas Ridge, displayed in the circulation diagrams of Figs. 15 and 16. Warm water north of 40°S flows westwards (25 Sv), as does intermediate water (7 Sv). This inflow is partly (or totally, for

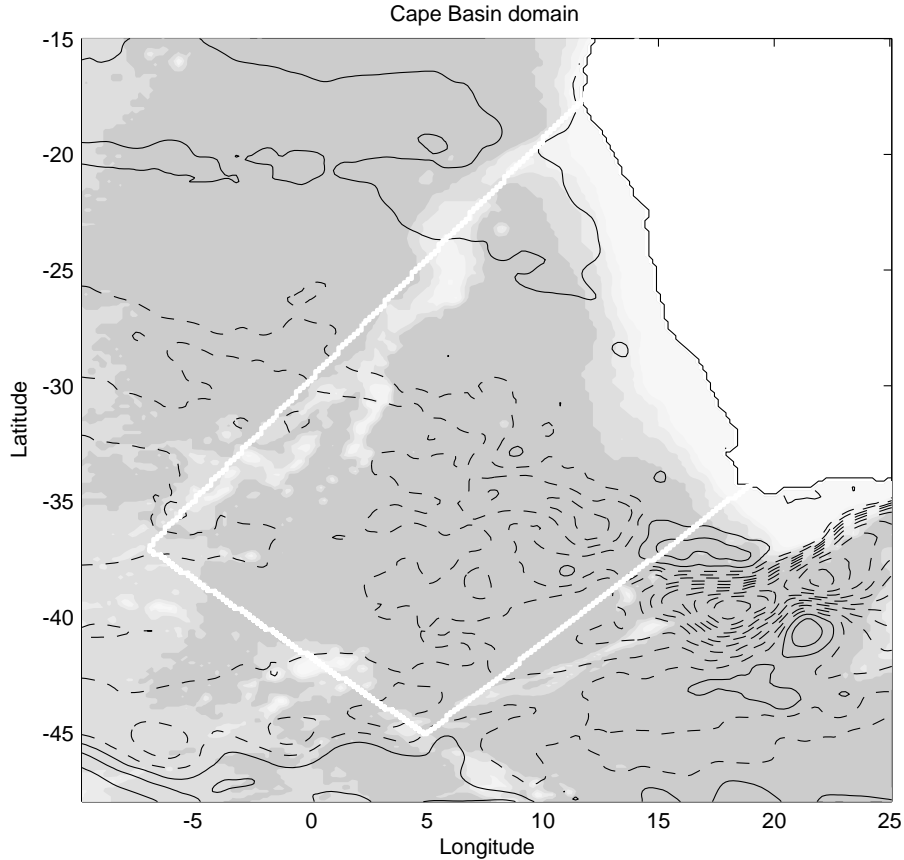


Fig. 14. Contours of the time-mean barotropic streamfunction (black lines) for years 1995–1999. Contour interval is 10 Sv; negative contours are dashed. The bottom topography is indicated in shades of grey, and the “Cape Basin” domain for the balances is outlined in white. Note that the contours of the domain exactly follow the boundaries of model grid cells.

the case of the intermediate water) compensated by an eastward return flow south of  $40^{\circ}\text{S}$ . This recirculation is explicitly presented in the summary figures for the circulation of warm and intermediate waters (Figs. 15 and 16). The inflow water is warm and salty, with fairly uniform properties. Rather than a front at  $40^{\circ}\text{S}$ , we find that the mean temperature and salinity decrease linearly from  $40^{\circ}\text{S}$  to  $46^{\circ}\text{S}$  along our section. This suggests that the waters just south of  $40^{\circ}\text{S}$  over the Agulhas Ridge resided for only a short time in the Cape Cauldron, without markedly altering their properties, while waters found at the southern end of the section might have stayed for a long time in the Cape Cauldron or even travelled all around the

subtropical gyre, experiencing a significant modification of their characteristics. Typical for a regime of turbulent mixing, all intermediate compositions exist between these two end numbers. Because of the intense eddy field, it seems difficult to quantify more precisely the importance of the different pathways; they are simply suggested as thin arrows in Figs. 15 and 16.

In the ATL6 model the volume in the four isopycnal layers is not conserved during the model integration, because the model is not in equilibrium with the forcing fields; the thermohaline circulation needs centuries to reach an equilibrium. During the course of the integration (28 years) the warm water volume increases at an

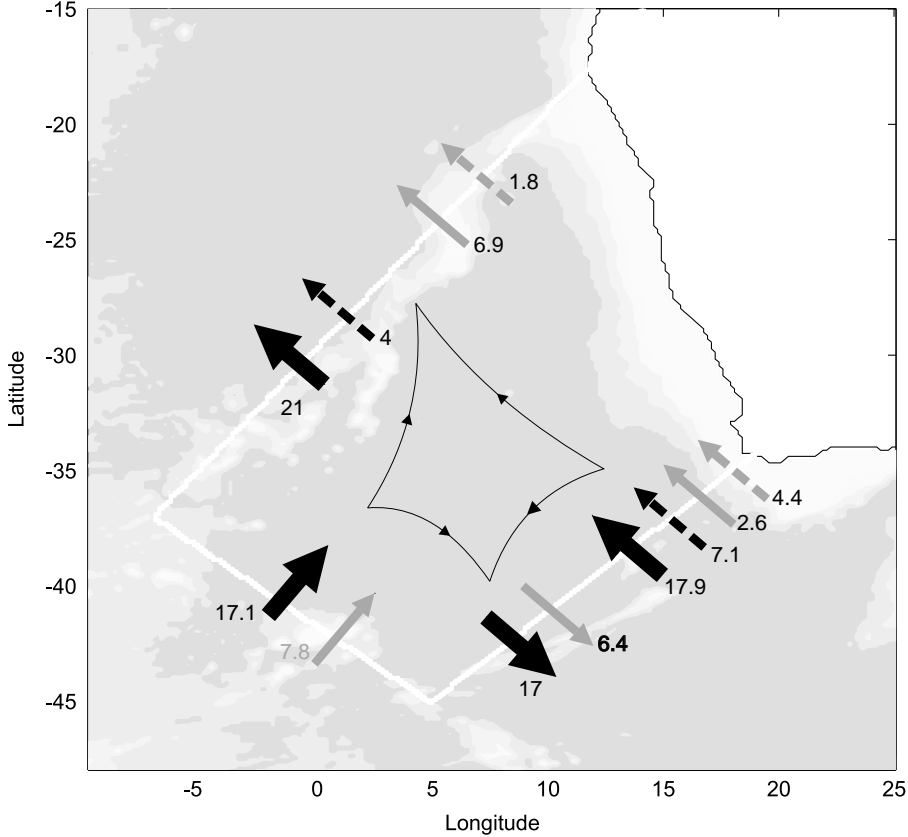


Fig. 15. Mass balance in the Cape Cauldron (in Sverdrups) for warm water (black arrows) and intermediate waters (grey arrows). The total mass flux is partitioned into the “trapped flux” in the rings (dashed arrows, see text for definition) and the “background” (plain arrows). We have not attempted to quantify the different water paths indicated qualitatively in the center of the domain.

average rate of 0.4 Sv, the intermediate and deep water volumes decrease (0.47 and 0.49 Sv, respectively), and the bottom water volume increases (0.56 Sv). The latter is certainly linked to the representation of bathymetry in the model: interpolated onto a  $1/6^\circ$  grid, the passage for Antarctic bottom water at the south of Walvis Ridge is too wide, so that the deep Angola Basin fills up with Antarctic bottom water. This problem did not exist in a low resolution version of the model, because interpolation on a  $1^\circ$  grid closed the passage completely.

The volume variations during the 5 years period considered here (1995–1999) are shown in Table 4. They are smaller than the long-term trends

mentioned above, sometimes reversed, and they are not monotonic over the 5 years. This demonstrates that after 20 years of integration the model (or forcing) systematic drifts have slowed enough to reach the order of magnitude of the interannual variability. The variations in volume are the result of the flux convergence into the box and diapycnal processes. Integrating the flux convergence from the bottom up and accounting for the drift in volume (Table 4), we find that the deep water converging into the box is mainly transformed into bottom water (at a rate of 1 Sv) while there is a small upwelling of deep water into intermediate water (0.3 Sv) and intermediate into warm water (0.1 Sv). Note that although the

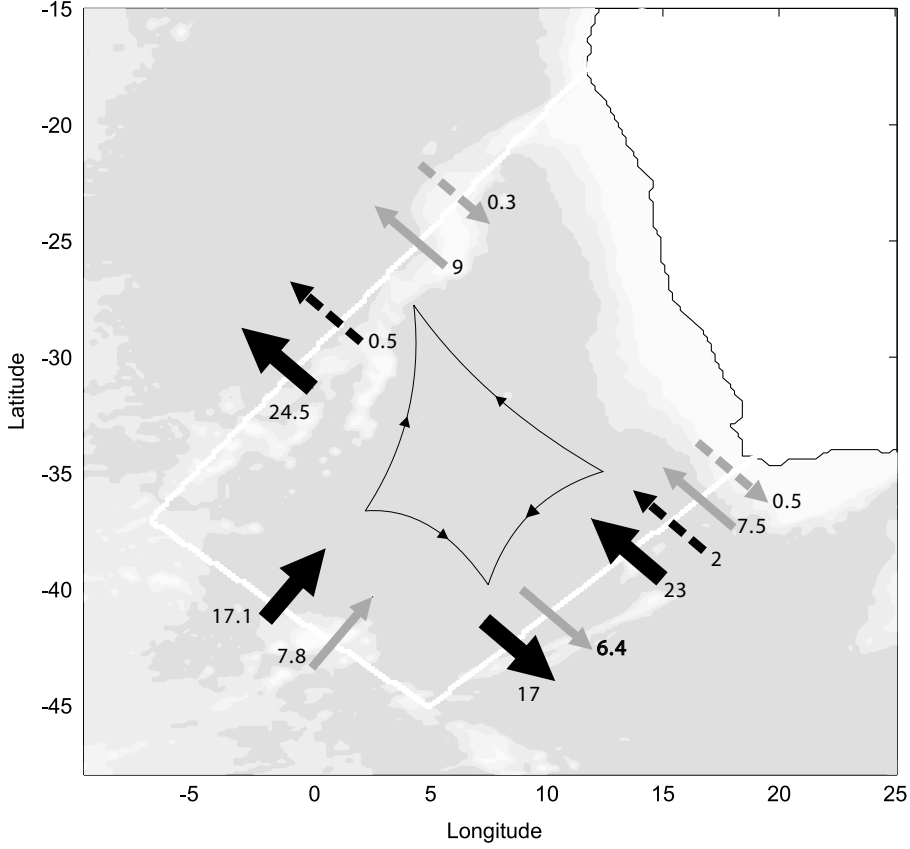


Fig. 16. Mass balance in the Cape Cauldron (in Sverdrups) for warm water (black arrows) and intermediate waters (grey arrows). The total mass flux is partitioned into the time mean flux (plain arrows) and the transient contribution (dashed arrows). We have not attempted to quantify the different water paths indicated qualitatively in the center of the domain.

Table 4

Mass fluxes (Sv) in the Cape Basin region, in the layers defined in Table 3. Fluxes are calculated for each model snapshot and averaged for years 1995–1999

Layer	West	Agulhas Ridge			Walvis Ridge			Flux convergence	$dV/dt$
		Total	$F'$	$F_t$	Total	$F'$	$F_t$		
WW	17.1	8.0	2.0	7.1	25.0	0.5	4.0	0.0	0.21
IW	7.8	0.6	-0.5	4.4	8.7	-0.3	1.8	-0.4	-0.22
DW	-1.7	-2.0	-0.3		-5.1			1.5	0.17
BW	-2.9	3.7	-1.2		2.0	-0.2		-1.1	-0.16
Total	20.3	10.3	0.0	11.5	30.6	0.0	5.8	0.0	0.0

The transient eddy contribution  $F'$  is indicated only when it exceeds 0.05 Sv. The “trapped” eddy contribution  $F_t$  is estimated for the warm water and intermediate water only, and defined as the contribution at grid points where the depth perturbation of isopycn  $\sigma_0 = 27$  is greater than 70 m. It has been omitted at the west section because it is very small (0.3 Sv). The total horizontal flux for each layer (flux convergence), as well as the volume variation of this layer  $dV/dt$  (averaged over the region for years 1995–1999) are also indicated. The difference between the two is due to water mass conversion by diffusion, and numerical errors.

model is not formulated in isopycnal coordinates, those cross isopycnal transfers are moderate. Mesoscale eddies are expected to mix water isopycnally, and it seems to be the case in the ATL6 model.

### 6.2. Eddy mass fluxes

Despite possible errors in the mean fluxes, ATL6 should give a realistic picture of the relative contribution of eddy fluxes. This contribution is indicated in Table 4 for both the transient and the “trapped” eddy flux, calculated using a criterion of depth anomaly larger than  $h_c = 70$  m.

As expected, the eddy component of the fluxes on the west section is negligible. On the other hand, the contribution of the rings is large across the Agulhas Ridge (Fig. 15). Because of the recirculation existing along this section, it looks like almost all the net flux of warm water across the Agulhas Ridge is accounted for by the flux trapped inside the eddies (7.1 out of 8 Sv). There is also a significant “trapped” flux of intermediate water associated with the rings (4.4 Sv) representing more than half the total inflow (7 Sv) north of 40°S along this section. Further downstream, above Walvis Ridge, the “trapped” fluxes are smaller by about 50%, showing that a significant amount of the volume associated with Agulhas

rings is mixed within the Cape Cauldron into the background flow.

The formulation of the fluxes in term of time-mean and transient (Fig. 16) shows a much smaller contribution from the turbulence, because as explained in the previous section most of the eddy effects are included in the mean flow. Across the Agulhas Ridge, the transient eddy flux of warm water  $F' = 2$  Sv is the same as observed at 30°S. The transient eddy fluxes of intermediate water have a sign opposite to the rings propagation: this is perhaps linked with the fact that the northward transient flux in the warm water layer must necessarily be compensated at depth at each location. The relatively small transient eddy contribution above Walvis Ridge is due to the fact that the rings are symmetric there and propagate uniformly.

### 6.3. Heat fluxes

Heat fluxes are indicated in Table 5. Salt fluxes (not shown) have a similar qualitative behavior.

The northward heat flux in the eastern South Atlantic (1.54 PW over Walvis Ridge from Table 5) is larger in ATL6 compared with lower resolution models like Reason et al. (2003): their value east of 5°E along 35°S is 1.02 PW only (1.34 PW in ATL6). Considering the total cross-basin heat

Table 5

Heat fluxes (PW) (or, when mass transport is non-zero, temperature fluxes referenced to 0°C). Fluxes are calculated from snapshots for years 1995–1999

Layer	West	Agulhas Ridge			Walvis Ridge			Flux convergence		$dH/dt$
		Total	$FH'$	$FH_t$	Total	$FH'$	$FH_t$	Total	$F'_c$	
WW	0.69	0.65	0.14	0.43	1.39	0.01	0.23	-0.04	0.13	0.02
IW	0.16	0.03	-0.01	0.10	0.2	-0.01	0.04	0.0	-0.01	0.0
DW	-0.01	-0.02			-0.06	0.02		0.01		0.0
BW	-0.01	0.02	-0.01		0.01	-0.01		-0.01	-0.01	0.0
Total	0.82	0.68	0.12	0.53	1.54	-0.04	0.27	-0.04	0.11	0.02

$dH/dt$  is the rate of variation of the box heat content during the period. The transient eddy heat flux  $FH'$  is indicated where it exceeds 0.01 PW. The “trapped” eddy contribution  $FH_t$  is estimated for the warm water and intermediate water only, and defined as the contribution at grid points where the depth perturbation of isopycn  $\sigma_0 = 27$  is greater than 70 m. For the flux convergence, both the total and the transient eddy contribution  $F'_c$  are indicated because (contrary to the mass fluxes) the vertical integral of the transient heat flux convergence does not vanish (it is quite large, 0.11 PW). The total heat flux into the surface of the box (from the atmosphere) is 0.06 PW: The heat content variation (0.02 PW) is the sum of the surface flux and the total flux convergence (-0.04 PW).

transport, the situation is reversed: 0.44 PW for ATL6 but 0.8 PW for the lower resolution model (Reason, personal communication). This happens because the subtropical gyre circulation (including the western boundary current) is stronger in the higher-resolution model. The gyre transports heat polewards and reduces the equatorward transport due to the thermohaline cell.

Contrary to the transient mass fluxes  $F'$ , which vanish when integrated over the water depth, the transient heat fluxes  $FH'$  have a net contribution. It is 0.12 PW over the Agulhas Ridge, a significant portion of the total and comparable to the transient eddy heat flux integrated over the 30°S cross-basin section.

The “trapped” eddy heat fluxes are large, but it is due to our definition: our heat fluxes are referenced to 0°C, while in most estimates from observations fluxes are calculated relative to the temperature of the background waters. Since the definition of “background” changes from a section to the next, we have chosen a common reference to make all numbers comparable.

The overall balance of the Cape Basin region for years 1995–1999 is a surface heating of 0.06 PW, balanced by a divergence of horizontal heat flux (−0.04 PW) and an increase of the heat content (at a rate of 0.02 PW). The surface heat flux is the sum of the applied ECMWF flux (0.1 PW) and the model-calculated retroaction term (−0.04 PW) due to the fact that the model SST is larger in average than observed SST; part of that feedback is probably due to the Agulhas rings.

Transient eddy heat fluxes produce a net convergence of heat into the region, and thus reinforce (rather than balance) the surface heating. However, as we have shown, transient fluxes reflect only part of the eddies’role, the other part being included in the mean fluxes. Since Agulhas rings produce transient fluxes over the Agulhas Ridge but much less over Walvis Ridge, a net transient flux convergence in the Cape Basin is expected. Similarly, there is a convergence of the trapped flux because Agulhas rings loose heat while crossing the Cape Basin. In the ATL6 model, the Benguela Current (northwards mean flow over Walvis Ridge, including a rectified eddy

contribution) is the main sink of heat for the Cape Basin.

## 7. Discussion

ATL6 offers the first opportunity to compare quantitatively two different points of view on the contribution of Agulhas eddies to the circulation of the Atlantic Ocean. Partitioning the total fluxes between “background” and “trapped eddy fluxes” emphasizes more the role of the Agulhas rings than the traditional partition between “time-mean” and “transient eddy fluxes”. Calculation of “trapped” eddy fluxes evidences the transport by eddies across a section, even when the eddies are symmetric and do not generate any transient flux.

Focussing on transient eddy fluxes is, in some sense, a weakness for eddy parameterization theories. Both the ATL6 model, and the simple thought experiment of an uniformly advected symmetric eddy, show that in many cases the eddies modify the mean property fluxes without generating any transient eddy flux. Such behavior has also been noted by Matano and Beier (2003) and Reason et al. (2003) in model studies of the Agulhas region. This makes it difficult to study the effect of mesoscale turbulence by considering only the usual transient eddy fluxes, either conceptually or by diagnostics from high-resolution numerical models.

However, the “trapped” eddy flux does not seem a viable alternative as a basis for parameterizations. First, as noted above, a calculation of the volume effectively “trapped” in the rings involves a Lagrangian calculation, extremely difficult to carry out accurately. In the present paper, as in previous estimates based on data, we have used an arbitrary criterion to define the “trapped” volume. But the largest obstacle to parameterization is probably the difficulty to achieve a formulation consistent with the requirements of energy and mass conservation in the model. The parameterization of transient eddy fluxes proposed by Gent et al. (1995) meets those consistency requirements. It is based on an “eddy induced velocity”, which is non-divergent (hence conserving mass), and its

definition ensures that it is a net sink of available potential energy for the mean flow. However, being a local parameterization it fails to represent the transport by a coherent eddy away from its region of generation.

## 8. Conclusion

The ATL6 model, despite its being a limited-area model with an open boundary south of Africa at 30°E, has been shown to generate a realistic variability in the Agulhas region. The eddy kinetic energy, the number, size and life time of the Agulhas rings compare well with observations. The fact that this happens in a model without any influence from Indian Ocean variability suggests that this influence is of a lesser degree than previously thought.

The model allows us to compare the ring propagation speed with the background Eulerian flow. This shows that the self-propagation of the rings is of the same order of magnitude as the advection by the mean flow, and in the same northwestward direction. The best fit between ring propagation and model Eulerian velocity is obtained with the velocity at a depth of 230 m. Contrary to idealized models, and especially quasi-geostrophic models, the rings in ATL6 do not interact strongly with the topography. Both in the data and in ATL6, eddy trajectories undergo a strong transition between a turbulent behavior in the Cape Basin and a steady propagation to the northwest afterwards. In the model however this transition seems due to eddy decay away from the generation region rather than to the direct influence of Walvis Ridge. Noticeable differences between the model and observations exist: the model Agulhas rings may be too shallow and drift too much equatorward in the western part of the South Atlantic Basin. Comparison with other high resolution models in the future could help understand the source of those discrepancies.

Because of its high spatial resolution ATL6 has allowed a first exploration of the nature of the cyclones recently observed in the Cape Basin (Boebel et al., 2003a). In ATL6 the cyclones are

mainly formed in the negative shear vorticity region of the Agulhas Current as suggested by the model of Penven et al. (2001), although other formation regions exist (for instance along the western boundary upwelling regime). The inflow at the model eastern boundary is fixed, but variability at seasonal and higher frequencies develop in the model Agulhas Current in response to local forcing as well as due to flow instabilities. Thus, this variability (especially on the inshore side) may play a part in the development of flow instabilities leading to cyclones in the model, as seems to happen in the real Agulhas Current (Lutjeharms et al., 2003). In both the ATL6 model and the MODAS SSH data, cyclones decay much more rapidly than anticyclones. In ATL6, they are rarely isolated but paired with the anticyclones in dipolar or tripolar structures. Because of their short life time and complicated evolution (they are often elongated as filaments) it seems reasonable to assume that they cannot carry water far from their source as anticyclonic rings do. On the other hand, their preferred formation region suggests that most cyclones contain initially water of Indian ocean origin, so that their decay is an efficient mixing mechanism for this water in the Cape Cauldron.

We have calculated the contribution of the eddies to the fluxes of mass and heat in ATL6. The fluxes themselves may be subject to errors of the model, its boundary conditions, and the forcing, but we believe that ATL6 gives a realistic picture of the *relative* influence of eddies. Across the Agulhas Ridge, the model shows an inflow into the Cape Cauldron of warm (25 Sv) and intermediate water (7 Sv) north of 40°S, at least half of which is due to water trapped in rings. This inflow is compensated by an eastward background flow of 18 Sv of warm water and 7 Sv of intermediate water, south of 40°S. This background return flow is partly made up of water having circulated around the subtropical gyre and partly of warm and salty waters from the Cape Cauldron itself. In the real ocean, the latter background flow has been exemplified by eight floats which had been launched in the Atlantic along the Southern boundary of the Cape Basin (to the northwest of the Agulhas retroflexion) and subsequently

became trapped by the Agulhas return current (Boebel et al., 2003b). This motion represents a transfer from the Atlantic to the Indian ocean, in opposition to what one would anticipate from past studies. Illustrations of two of these floats (# 195 and # 196) are given in Lutjeharms et al. (2003). Farther northwest, over Walvis Ridge, the ATL6 model is in agreement with the inverse model estimate of Sloyan and Rintoul (2001) for the division between the warm and intermediate water transport, although the total transport is larger in the model.

ATL6 shows important transient eddy fluxes over the Agulhas Ridge and across the 30°S section. The transient heat flux  $\overline{v'T'}$  across 30°S is 0.11 PW, 25% of the total. It was much smaller in a lower resolution version of the model (Treguier et al., 2001). By comparing two approaches to quantify the eddy contribution, we have shown that the presence of eddies does not necessarily lead to important transient eddy fluxes (or eddy-induced velocities). Where those fluxes exist in the model however, they would imply very large mixing coefficients if using existing parameterizations (a coefficient of 10 000 m<sup>2</sup> s<sup>-1</sup> at 30°S with the parameterization of Gent et al., 1995).

The complex and fascinating behavior of oceanic turbulence in the Cape Cauldron promises many more interesting studies, both observationally and theoretically. This region of the world ocean is perhaps a hopeless challenge for parameterizations, because eddies generated at the Agulhas retro-reflection transport water and energy away from their source, so that any local parameterization will necessarily fail. It is quite possible that the spatial resolution of future climate models will be dictated by the need to resolve Agulhas eddies in order to represent accurately the Atlantic–Indian interocean exchange.

## Acknowledgements

This study was made possible by Jean Marc Molines and Anne de Pimenta who managed the CLIPPER 1/6° model, and Sylvain Michel who wrote the diagnostic programs. We thank Charlie Barron (Naval Research Laboratory, Stennis

Space Center, USA) for providing MODAS data, and Michel Arhan for useful suggestions. The CLIPPER model was run at the IDRIS computer center in Orsay, France. The CLIPPER project is funded by various French government agencies: CNRS, IFREMER, CMO, CNES and Météo-France.

## References

- Arhan, M., Mercier, H., Lutjeharms, J.R.E., 1999. The disparate evolution of three Agulhas rings in the South Atlantic Ocean. *Journal of Geophysical Research* 104, 20987–21005.
- Barnier, B., Siefridt, L., Marchesiello, P., 1995. Thermal forcing for a global ocean circulation model using a three-year climatology of ECMWF analyses. *Journal of Marine Systems* 6, 363–380.
- Barnier, B., Marchesiello, P., de Miranda, A.P., Molines, J.M., Coulibaly, M., 1998. A sigma-coordinate primitive equation model for studying the circulation in the South Atlantic. Part I: Model configuration with error estimates. *Deep-Sea Research I* 45, 543–572.
- Beismann, J.O., Kase, R., Lutjeharms, J.R.E., 1999. On the influence of submarine ridges on translation and stability of Agulhas rings. *Journal of Geophysical Research* 104, 7897–7906.
- Biastoch, A., Krauss, W., 1999. The role of mesoscale eddies in the source regions of the Agulhas current. *Journal of Physical Oceanography* 29, 2302–2317.
- Boebel, O., Barron, C., 2003. A comparison of in-situ float velocities with altimeter derived geostrophic velocities. *Deep-Sea Research II*, this issue (PII: S0967-0645(02)00381-8).
- Boebel, O., Lutjeharms, J.R.E., Rossby, T., Zenk, W., 2003a. The Cape Cauldron: an Agulhas mixing and exchange regime. *Deep-Sea Research II*, this issue (PII: S0967-0645(02)00379-X).
- Boebel, O., Rossby, T., Lutjeharms, J.R.E., Zenk, W., 2003b. Path and variability of the Agulhas return current. *Deep-Sea Research*, this issue (PII: S0967-0645(02)00377-6).
- Carton, X., Legras, B., 1994. The life-cycle of tripoles in two-dimensional incompressible flows. *Journal of Fluid Mechanics* 267, 53–82.
- CLIPPER project team, 2000. 1/6° Atlantic circulation model forced by the ECMWF climatology: preliminary results. LPO report 00-01, 130pp. Available at [www.ifremer.fr/lpo/clipper](http://www.ifremer.fr/lpo/clipper).
- CLIPPER project team, 2001. High resolution modelling of the Atlantic circulation, final report, CLIPPER-R1-20001, Laboratoire des Ecoulements Géophysiques et industriels, Grenoble, 144pp.
- Dewar, W.K., Killworth, P.D., 1995. On the stability of oceanic rings. *Journal of Physical Oceanography* 25, 1467–1487.
- Dewar, W.K., Killworth, P.D., Blundell, J.R., 1999. Primitive-equation instability of wide oceanic rings. Part II:

- numerical studies of ring stability. *Journal of Physical Oceanography* 29, 1744–1758.
- Ducet, N., Le Traon, P.Y., Reverdin, G., 2000. Global High resolution of ocean circulation from TOPEX/Poseidon and ERS1/2. *Journal of Geophysical Research* 105, 19477–19498.
- Fox, D.N., Teague, W.J., Barron, C.N., Carnes, M.R., Lee, C.M., 2001. The Modular Ocean Data Assimilation System (MODAS). *Journal of Atmospheric Oceanic Technology* 19, 240–252.
- Garnier, E., Verron, J., Barnier, B., 2002. Variability of the South Atlantic upper ocean circulation: a data assimilation experiment with 5 years of TOPEX/POSEIDON altimeter observations. *International Journal of Remote Sensing*, in press.
- Garzoli, S.L., Gordon, A.L., Kamenkovich, V., Pillsbury, D., Duncombe Rae, C.M., 1996. Variability and sources of the southeastern Atlantic circulation. *Journal of Marine Research* 54, 1039–1071.
- Garzoli, S.L., Richardson, P.L., Duncombe Rae, C.M., Fratantoni, D.M., Goñi, G.J., Roubicek, A.J., 1999. Three Agulhas rings observed during the Benguela Current Experiment. *Journal of Geophysical Research* 104, 20971–20985.
- Gent, P.R., Willebrand, J., McDougall, T.J., McWilliams, J.C., 1995. Parameterizing eddy-induced tracer transports in ocean circulation models. *Journal of Physical Oceanography* 25, 463–474.
- Goñi, G.J., Garzoli, S.L., Roubicek, A.J., Olson, D.B., Brown, O.B., 1997. Agulhas ring dynamics from TOPEX/Poseidon satellite altimeter data. *Journal of Marine Research* 55, 861–883.
- Kamenkovich, V.M., Leonov, Y.P., Nachaev, D.A., Byrne, D.A., Gordon, A.L., 1996. On the influence of bottom topography on the Agulhas eddy. *Journal of Physical Oceanography* 26, 892–912.
- Lutjeharms, J.R.E., Webb, D.J., 1995. Modelling the Agulhas current system with FRAM (Fine Resolution Antarctic Model). *Deep Sea Research* 42, 523–551.
- Lutjeharms, J.R.E., Boebel, O., Rossby, T., 2003. Agulhas cyclones. *Deep Sea Research II*, this issue (PII: S0967-0645(02)00378-8).
- Madec, G., Delecluse, P., Imbard, M., Levy, C., 1998. OPA 8.1 general circulation model reference manual, Notes de l'IPSL, Universit P. et M. Curie, B102 T15-E5, 4 place Jussieu, Paris cedex 5, N 11, 91p.
- Maltrud, M.E., Smith, R.D., Semtner, A.J., Malone, R.C., 1998. Global eddy-resolving ocean simulations driven by 1985–1995 atmospheric winds. *Journal of Geophysical Research* 103, C13, 30825–30853.
- Matano, R.P., Beier, E.J., 2003. A kinematic analysis of the Indian/Atlantic Inter-ocean exchange. *Deep-Sea Research II*, this issue (PII: S0967-0645(02)00395-8).
- McDonagh, E.L., Heywood, K.J., Meredith, M.P., 1999. On the structure, paths and fluxes associated with Agulhas Rings. *Journal of Geophysical Research* 104, 21007–21020.
- Mc Williams, J.C., Flierl, G.R., 1979. On the evolution of isolated, nonlinear vortices. *Journal of Physical Oceanography* 9, 1155–1182.
- Olson, D.B., Evans, R.H., 1986. Rings of the Agulhas Current. *Deep-Sea Research* 33, 1–42.
- Park, Y.H., Charriaud, E., Craneguy, P., Kartavtseff, A., 2001. Fronts, transport and Weddell Gyre at 30°E between Africa and Antarctica. *Journal of Geophysical Research* 106, 2857–2879.
- Penduff, T., Barnier, B., Beranger, K., Verron, J., 2001. Comparison of near-surface mean and eddy flows from two numerical models of the South Atlantic Ocean. *Journal of Geophysical Research* 106, 16857–16867.
- Penven, P., Lutjeharms, J.R.E., Marchesiello, P., Roy, C., Weeks, S.J., 2001. Generation of cyclonic eddies by the Agulhas current in the lee of the Agulhas bank. *Geophysical Research Letters* 28, 1055–1058.
- Pichevin, T., Nof, D., Lutjeharms, J.R.E., 1999. Why are there Agulhas rings? *Journal of Physical Oceanography* 29, 693–707.
- Reason, C.J.C., Lutjeharms, J.R.E., Hermes, J., Biastoch, A., Roman, E.R., 2003. Inter-ocean fluxes south of Africa in an eddy permitting model. *Deep-Sea Research II*, this issue.
- Reynaud, T., Legrand, P., Mercier, H., Barnier, B., 1998. A new analysis of hydrographic data in the Atlantic and its application to an inverse modelling study. *International WOCE Newsletter*, Number 32, 29–31.
- Rintoul, S., 1991. South Atlantic inter-basin exchange. *Journal of Geophysical Research* 96, 2675–2692.
- Schmid, C., Siedler, G., Zenk, W., 2000. Dynamics of intermediate water circulation in the subtropical South Atlantic. *Journal of Physical Oceanography* 30, 3191–3211.
- Schmid, C., Boebel, O., Zenk, W., Lutjeharms, J.R.E., Garzoli, S., Richardson, P.L., Barron, C., 2003. Early evolution of an Agulhas ring. *Deep-Sea Research II*, (PII: S0967-0645(02)00382-X).
- Schouten, M.W., de Ruijter, W.P.M., van Leeuwen, P.J., 2000. Translation, decay and splitting of Agulhas rings in the southeastern Atlantic Ocean. *Journal of Geophysical Research* 105, 21913–21925.
- Sloyan, B.M., Rintoul, S.R., 2001. Circulation, renewal and modification of Antarctic mode and intermediate water. *Journal of Physical Oceanography* 31, 1005–1030.
- Smith, W.H.F., Sandwell, D.T., 1997. Global Seafloor topography from Satellite Altimetry and ship depth soundings. *Science* 277, 1956–1962.
- Smith, R.D., Maltrud, M.E., Bryan, F.O., Hecht, M.W., 2000. Numerical simulation of the North Atlantic Ocean at 1/10°. *Journal of Physical Oceanography* 30, 1532–1561.
- Sparrow, M.D., Boebel, O., Zervakis, V., Zenk, W., Cantos-Figuerola, A., Gould, W.J., 2002. Two circulation regimes of the mediterranean outflow revealed by hagrangian measurements. *Journal of Physical Oceanography* 32 (5), 1322–1330.

Treguier, A.M, Barnier, B., de Miranda, A.P., Molines, J.M., Grima, N., Imbard, M., Madec, G., Messenger, C., Reynaud, T., Michel, S., 2001. An eddy permitting model of the Atlantic Circulation: evaluating open boundary conditions. *Journal of Geophysical Research* 106, 22115–22129.

van Ballegooyen, R.C., Grundlingh, M.L., Lutjeharms, J.R.E., 1994. Eddy fluxes of heat and salt from the southwest Indian Ocean into the southeast Atlantic ocean: a case study. *Journal of Geophysical Research* 99, 14053–14070.